# The role of tides in the spreading of Mediterranean Outflow waters along the southwestern Iberian margin

Alfredo Izquierdo[a,*], Uwe Mikolajewicz[b]

[a] *Applied Physics Department, University of Cádiz, CEIMAR, Cádiz, Spain, Avda. República Saharahui s/n, CASEM 11510, Puerto Real, Cádiz, Spain*
[b] *Max Planck Institute for Meteorology, Hamburg, Germany, Bundesstraße 53, Hamburg 20146, Germany*

A B S T R A C T

The impact of tides on the spreading of the Mediterranean Outflow Waters (MOW) in the Gulf of Cadiz is investigated through a series of targeted numerical experiments using an ocean general circulation model. The full ephimeridic luni-solar tidal potential is included as forcing. The model grid is global with a strong zoom around the Iberian Peninsula. Thus, the interaction of processes of different space and time scales, which are involved in the MOW spreading, is enabled. This is of particular importance in the Strait of Gibraltar and the Gulf of Cádiz, where the width of the MOW plume is a few tens of km. The experiment with enabled tides successfully simulates the main tidal features of the North Atlantic and in the Gulf of Cádiz and the Strait of Gibraltar. The comparison of the fields from simulations with and without tidal forcing shows drastically different MOW pathways in the Gulf of Cádiz: The experiment without tides shows an excessive southwestward spreading of Mediterranean Waters along the North African slope, whereas the run with tides is closer to climatology. A detailed analysis indicates that tidal residual currents in the Gulf of Cádiz are the main cause for these differences.

## 1. Introduction

The narrow (~14 km) and rather shallow (~300 m at the main sill) Strait of Gibraltar (SoG) is the only connection between the Mediterranean Sea and the North Atlantic (NA) Ocean. Lighter Atlantic waters enter the Mediterranean Sea as a surface flow and spread out through the Western and Eastern Mediterranean basins while being modified gradually by mixing with the underlying waters. The density of these surface waters increases due to evaporation and cooling. Finally they form the saline and warm intermediate and deep Mediterranean Waters, which in turn flow into the Atlantic Ocean as an undercurrent through the SoG at a rate of approximately 1 Sv ($10^6$ m$^3$ s$^{-1}$). Once in the Gulf of Cadiz (GoC), the Mediterranean Outflow Water (MOW) descends gradually to its equilibrium depth (~1000 m) flowing westward along the Iberian continental slope while entraining overlying North Atlantic Central Waters (NACW). The result is the formation of the Mediterranean Water that finally spreads into the interior of the NA forming the most prominent basin-scale thermohaline anomaly at mid-depths: the Mediterranean salt tongue (Fig. 1). In this work we will focus primarily in the GoC, therefore we will use the acronym MOW independently of the degree of transformation of the pure outflow water.

The fate of MOW involves a wide range of spatial and temporal scales. This is most evident at the SoG and in the GoC, where the MOW core has a width of just a few tens of km. Changes in the characteristics

of Atlantic and/or Mediterranean water masses could affect the exchange flows through the SoG, and also the fluxes of salt, heat and other properties. These changes may be induced by atmospheric disturbances (e.g., Garrett et al., 1989; Candela et al., 1989), seasonal cycles (Bormans et al., 1986), and interannual, decadal or longer climate variability (Brandt et al., 2004).

Superimposed on these exchange flows, a strong tidal forcing acts in the SoG (Candela et al., 1990). This substantially modifies the amount of exchanged salt and water due to the high correlation over the tidal period between the depth of the interface and the strength of the inflowing currents (Bryden et al., 1994). This oscillatory flow, in turn, interacts with the main sill of the strait creating an internal bore of high amplitude, which further propagates and disintegrates into a train of internal solitary waves (e.g. Brandt et al., 1996; Izquierdo et al., 2001; Sánchez-Garrido et al., 2008; 2011; Vlasenko et al., 2009). These internal waves provide energy for mixing in the SoG, and they are likely to determine to some extent the volume and characteristics of the MOW. In the GoC, the local scale processes also are supposed to play an important role, for example through the effect of submarine canyons and banks over the MOW undercurrent (Serra et al., 2005). These bottom topography features also interact with the tidal flow generating internal waves and affecting tidally induced mixing and residual currents (Bruno et al., 2006; Quaresma and Pichon, 2013). A recent analysis of near-bottom high resolution CTD and velocity data at the GoC (Sánchez-Leal et al., 2017) shows the impact of mean flow-topography

---
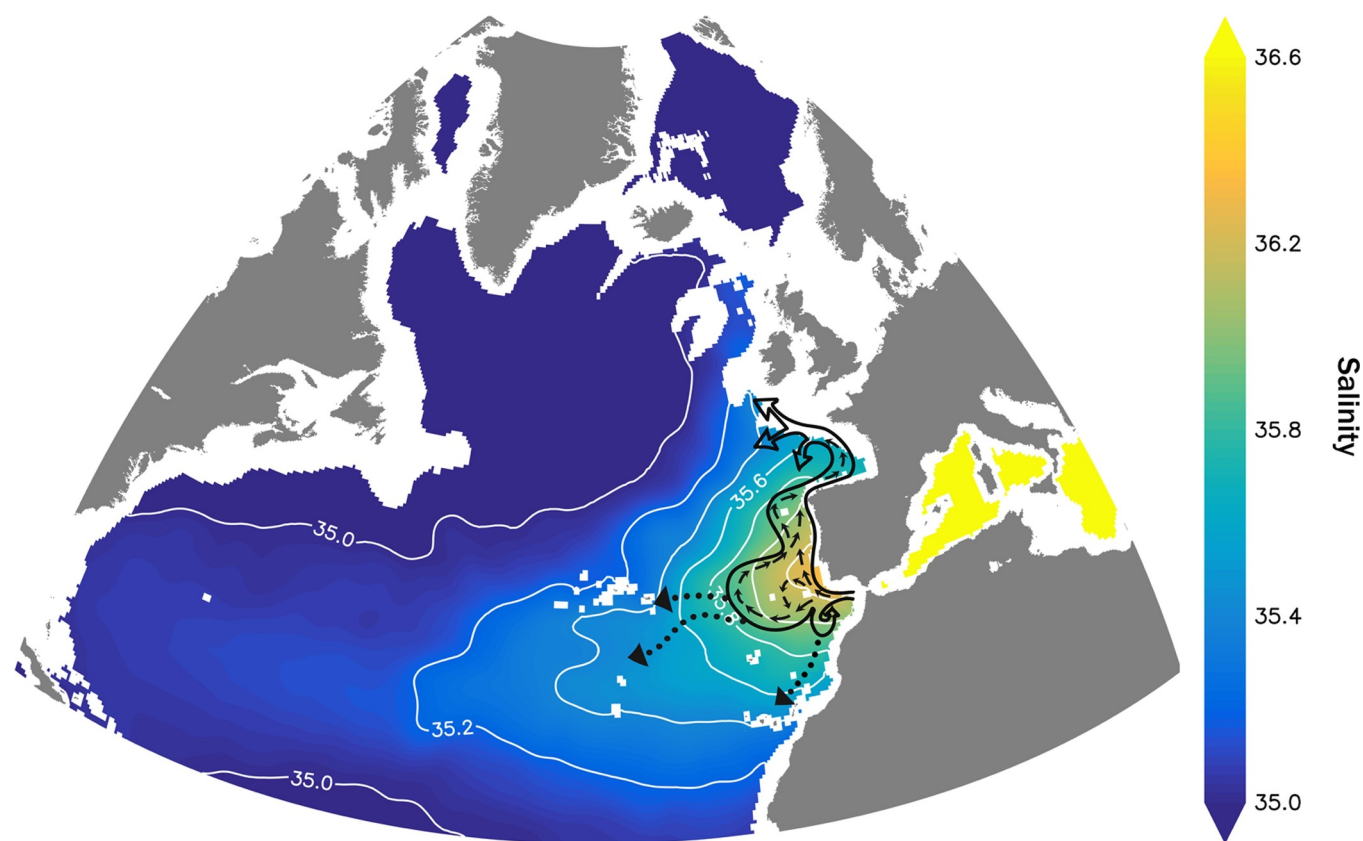
**Fig. 1.** Mediterranean Salt Tongue representation on the World Ocean Atlas 2013 (WOA13, Zweng et al., 2013) salinity field at 1200 m depth. The overlaid scheme (modified after Iorga and Lozier, 1999a) indicates the permanent MOW pathways (continuous arrows) and the preferred paths of meddies (dotted arrows).

interaction on the fate of MOW along the GoC, but, to our knowledge, the impact of the tide-topography interaction on the MOW undercurrent has been never considered.

Based on observational evidence, there is a good understanding of the behaviour of the MOW in the vicinity of the GoC. The general picture, excellently summarized by Iorga and Lozier (1999a), is that MOW moves westward as a wall-bounded undercurrent by the Iberian continental slope. Most MOW passes through the 'gateway' between S. Vicente Spur and Gorringe Bank (e. g., Zenk and Armi, 1990; Daniault et al., 1994; Iorga and Lozier, 1999a, 1999b; Bower et al., 2002; Carracedo et al., 2014) and then moves northward as a poleward eastern boundary undercurrent. Another branch of MOW recirculates cyclonically in the GoC (Daniault et al., 1994; Iorga and Lozier, 1999a,b; Bower et al., 2002) (see Fig. 1). Meddies (or Mediterranean eddies, isolated rotating lenses of warm salty Mediterranean Water) play also an important role for the propagation of MOW properties to the ocean interior (Bower et al., 2002). This transport is directed generally towards southwest (Richardson et al., 1991; Iorga and Lozier, 1999a; Bower et al., 2002).

Most of the modelling work on MOW has been done with limited area models in the vicinity of the SoG and the GoC, starting from the pioneering works by Jungclaus and Mellor (2000), who used the POM model for a MOW process study excluding any external forcing, and Johnson and Stevens (2000) and Johnson et al. (2002), who used a model based on MOM (Modular Ocean Model, Pacanowski et al., 1990) specifying barotropic streamfunction and partly tracer relaxation at open boundaries. However none of them included tides as a factor with possible influence in MOW spreading in the GoC. The relevance of flow/topography interaction in the GoC for MOW spreading has been established (Sánchez-Leal et al., 2017), but the tidal contribution to topographically induced processes has been disregarded.

From the point of view of tidal dynamics, the GoC is a very

interesting region, as it is influenced by the different tidal regimes of the NA and the SoG. Quaresma and Pichon (2013) found small-scale variability of the tidal harmonic solutions over the shelf and over nearby seamounts caused by the generation of diurnal continental shelf waves and topographic modulation of the semi-diurnal tidal ellipses. Along-shelf, the semi-diurnal velocities show higher spatial variability than the amplitudes of sea surface elevation. Over the major shelf-width anomalies (as submarine canyons and promontories), the tidal current is magnified and changes the rotation sense to anti-cyclonic. The same behaviour is observed around Cape S. Vicente as well as over the nearby seamounts (Gorringe). Quaresma and Pichon (2013) also reported strong internal tide activity in some located 'hotspots'.

The goal of this paper is to investigate the role of tides for the spreading of the MOW in the Gulf of Cadiz and along the southwestern Iberian margin. In order to do so, we apply a global ocean model with a strong focus on the region of interest. The paper is organized as follows: The model setup is presented in Section 2. The numerical experiments and results are provided in Section 3, while Section 4 contains the discussion of the results.

## 2. Model setup

We employ a special setup of the Max Planck Institute Ocean Model (MPIOM), developed at the Max Planck Institute for Meteorology (Maier-Reimer, 1997; Marsland et al., 2003; Jungclaus et al., 2013) which allows us to use a global model with a strong zoom on the SoG and the GoC. MPIOM is a free surface, primitive equations ocean model, which uses the Boussinesq and incompressibility approximations. The model is formulated on an orthogonal curvilinear Arakawa C-grid with vertical discretization on z-levels. The curvilinear grid allows for the placement of the poles over land, thus removing the numerical singularity associated with convergence of meridians at the geographical

poles. One important advantage of the curvilinear grid is that high resolution in the region of interest can be reached by adequate positioning of the model grid poles, while maintaining a global domain. Vertical mixing and diffusion are formulated depending on the Richardson number according to Pacanowski and Philander (1981). A simple mixed layer scheme is included. Convection in case of unstable stratification is treated by enhanced vertical diffusion (Marsland et al., 2003). A bottom boundary layer (BBL) slope convection scheme was included, which allows for a better representation of the flow of statically unstable dense water masses over sills and off shelves (Marsland et al., 2003). Lateral diffusion of the tracer fields is done using an isopycnal scheme (Griffies, 1998). Unresolved eddy-induced tracer transport has been included by the implementation of a Gent and McWilliams style parameterization (Gent et al., 1995). Advection of scalar tracers is computed with a second-order total variation-diminishing scheme (Sweby, 1984). Tides can be calculated by prescribing the full ephimeridic luni-solar tidal potential (Thomas et al., 2001).

### 2.1. Grid configuration

As this study focuses on the MOW and its spreading from the SoG along the southwestern Iberian margin, the model grid has very high resolution along the coast of the Iberian Peninsula and gradually decreasing resolution elsewhere. The model is global, which allows us to combine the high spatial resolution required in key regions for the Mediterranean overflow and subsequent spreading in the GoC, and the large scales required for the subsequent spreading in the NA. This approach avoids one of the most prominent problems of regional ocean models, the specification of boundary values in the ocean interior. The grid configuration used in this study (SPAN10, Fig. 2) places one pole in the Iberian Peninsula (at 4.7°W and 39.25°N), the other in South America (4°S, 89°W), allowing 4 km resolution at the SoG (formal mean global resolution 1.0°). The SPAN10 setup combines the explicit exchange through a realistic SoG and tidal forcing, as well as a realistic representation of the most relevant topographic features in the SoG and the GoC (Fig. 2) essential for the spreading of the MOW (Sánchez-Leal et al., 2017).

The model has 80 vertical levels with level thickness increasing with depth (centered at 8, 21, 31, 41, 51, 61, 71, 81, 91, 101, 111, 121, 131, 141, 151, 161, 171, 181, 191, 201, 211, 221, 231, 242, 254, 267, 281,

296, 312, 329, 347, 366, 386, 407, 429, 452, 476, 501, 527, 554, 582, 611, 641, 672, 704, 737, 771, 806, 842, 879, 918, 959, 1002, 1047, 1094, 1143, 1196, 1253, 1316, 1383, 1458, 1543, 1638, 1743, 1858, 1983, 2118, 2263, 2423, 2598, 2783, 2978, 3188, 3423, 3683, 3968, 4293, 4668, 5093, and 5568 m depth), allowing a fair vertical resolution and keeping the implicit vertical numerical diffusivity small. For an accurate temporal resolution of the tidal oscillations and to guarantee numerical stability, the model time step was 432 s.

The coefficients of horizontal friction/tracer diffusion in the model are formulated spatially varying depending on local grid resolution. The vertical mixing in the standard version was tuned to yield an optimal representation of the hydrography in the North Atlantic. Therefore we have decided to keep all model parameters near the standard values without fine-tuning the model, as our main objective is to study the effect of tides on the spreading of MOW.

Surface forcing was similar as described in Marsland et al. (2003). The OMIP climatology (Röske, 2001) was used for the atmospheric surface forcing. This data set combines the advantages of using the same forcing for every model year, while maintaining a realistic short-term variability on daily time scale. Heat fluxes and evaporation are calculated using bulk formula with prescribed atmospheric quantities and actual model sea surface temperature (SST). The only direct restoring term used in this model setup is surface salinity restoring to the PHC 2.1 climatology (Steele et al., 2001). The ocean initial state was taken from the same climatology. The parameter values employed in the MPIOM-SPAN10 runs are listed in Table 1.

## 3. Results

### 3.1. Baseline experiments

Two baseline experiments have been performed with the SPAN10 setup. In experiment TIDE the full ephimeridic luni-solar tidal potential was activated, in experiment NOTIDE it was not. This is the only difference between these two experiments. Both experiments were integrated for 13 years. This turned out to be sufficient to ensure that the oceanographic fields in the eastern NA reflect the model physics and not the initial conditions. A list of experiments can be found in Table 2.
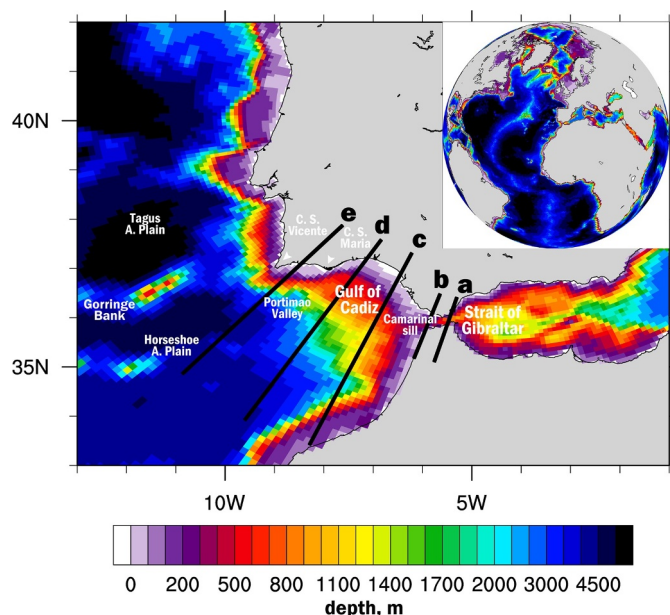


**Fig. 2.** MPIOM-SPAN10 grid and bathymetry around the Iberian Peninsula. Inset shows MPIOM-SPAN10 grid global view (colorbar indicates depth in metres). Black lines mark the cross-sections plotted in Fig. 9.

**Table 1**
Coefficient values employed in the MPIOM-SPAN10 setup.

| Symbol | Description | Value |
|---|---|---|
| $dt$ | Time step | 432 s |
| $A_b$ | Background vertical viscosity | $1.0 \times 10^{-4}\,\mathrm{m^2\,s^{-1}}$ |
| $A_{VO}$ | Richardson number dependent vertical viscosity | $5.0 \times 10^{-2}\,\mathrm{m^2\,s^{-1}}$ |
| $B_H$ | Biharmonic horizontal viscosity | $1.1 \times 10^{-8}\,\mathrm{s^{-1}}\,x\,(\Delta x^4, \Delta y^4)$ |
| $BBL_{MAX}$ | Maximum BBL thickness | 500 m |
| $D_b$ | Background vertical diffusivity | $2.0 \times 10^{-5}\,\mathrm{m^2\,s^{-1}}$ |
| $D_{VO}$ | Ricardson number dependent vertical diffusivity | $3.0 \times 10^{-2}\,\mathrm{m^2\,s^{-1}}$ |
| $D_H$ | Harmonic horizontal diffusion | $2.5 \times 10^{-3}\,\mathrm{m\,s^{-1}}\,x\,(\Delta x, \Delta y)$ |
| $B_{fl}$ | Linear bottom friction | $1.0 \times 10^{-3}\,\mathrm{m^2\,s^{-1}}$ |
| $B_{fq}$ | Quadratic bottom friction | $3.0 \times 10^{-3}$ |
| $C_{CON}$ | Vertical mixing for tracer convection | $0.5\,\mathrm{m^2\,s^{-1}}$ |

### 3.2. Tides in the global SPAN10

Müller et al. (2010) already demonstrated the ability of the global MPIOM to properly simulate ocean tides. The SPAN10 configuration of MPIOM also succeeds in depicting a satisfactory representation of the main tidal waves in the NA. For validation purposes, we performed a least square harmonic analysis of sea level on a 1-year long chunk of model output from experiment TIDE. Fig. 3a presents the simulated $M_2$ partial tide, which is the dominant tidal component in the North Atlantic. The agreement between MPIOM-SPAN10 $M_2$ tide and that obtained from accurate tidal models is reasonable in the NA for a climate model. This can be observed comparing the $M_2$ cotidal chart simulated by MPIOM-SPAN10 (Fig. 3a) to that obtained from the global high-resolution tidal model HAMTIDE (Taguchi et al., 2014) with data assimilation shown in Fig. 3b. The $M_2$ tide travels as a sort of Kelvin wave rotating counter-clockwise around the central NA amphidromic point. The increase in amplitude towards the northwestern European shelf and the Labrador Sea is properly represented. The amphidromic systems are well captured, especially in the central North Atlantic, the 3 major amphidromic systems of the North Sea (Southern Bight, German Bight and southwest Norwegian coast), the Iceland-Faroe Rise, the Denmark Strait, the Baffin Bay (west of Greenland) and the Gulf of St. Lawrence. Some of the amphidromic points are slightly shifted (the central North Atlantic is displaced to the northwest) causing in some cases their degeneration (Baffin Bay and Denmark Strait).

At the same time MPIOM-SPAN10 simulates key features of the tides in the GoC and the SoG in a realistic manner. Fig. 4 shows a detailed $M_2$ cotidal chart reproducing the two main features noted by Candela et al. (1990) from bottom pressure observations in the SoG: (i) The $M_2$ amplitude decreases by more than 50% from the Atlantic to the Mediterranean side but it is otherwise uniform across the strait, and (ii) in contrast, the lines of constant phase (cotidal lines) are mostly oriented east-west along the channel. Those features were confirmed by the high-resolution models of Tejedor et al. (1998, 1999) and Sannino et al. (2004). They found a two-fold west to east decrease in amplitudes and a southwestward propagation within the SoG, with a nearly 20° phase difference between Gibraltar and Cape Espartel (from NE to SW across

the strait) and a 10° north to south phase difference at the Atlantic side.

Therefore, the MPIOM-SPAN10 $M_2$ spatial structure (Fig. 4) is very close to that well known from tidal gauge data and tidal local models. Candela et al. (1990) already noticed that the $M_2$ phase propagation observed in Gibraltar is in clear opposition to the North Atlantic deep water tide west of the strait, which propagates northward, raising the question on the matching between both tidal patterns.

In our results the SoG acts as a source point but its influence is limited to the easternmost GoC. An area of nearly constant phases and amplitudes characterizes the central GoC. To the west of the GoC the $M_2$ tide becomes more progressive, diffracting around Cape S. Vicente and retaining maximum amplitude values at the head of the GoC, in accordance with Quaresma and Pichon (2013).

Fig. 5 displays a comparison of the simulated $M_2$ tidal current ellipse parameters with those obtained from two vertical arrays of four current-meters moored at the GoC (Instituto Español de Oceanografía, indamar.ieo.es) in the framework of the European project CANIGO. Two mooring arrays were located to the south of Cape S. Vicente at 36° 29′ N, 8° 51′ W and 36° 22′ N, 8° 49′ W, with a water depth of 2030 and 2880 m, respectively (see Fig. 6).

The full time series covers a period from 14/06/1997 to 21/08/1998 with hourly resolution, sufficient to perform a harmonic analysis for the characterization of the main tidal components. MPIOM-SPAN10 reasonably well simulates the observed vertical structure of the $M_2$ tidal currents. It slightly underestimates their small amplitude, but it properly reproduces the eccentricity of the tidal current ellipses (ratio of the semi-minor and semi-major axes), the sense of rotation (given by the sign of the semi-minor axis, negative - clockwise) and their vertical structure, with minimum amplitudes and an abrupt change of phases at intermediate (MOW) depths. In general, the model simulation adequately represents the effect of stratification on the vertical structure of the observed $M_2$ current velocities.

Fig. 6 shows the spatial distribution of the modelled depth-averaged $M_2$ tidal current ellipses in the GoC. Along strait, large amplitude tidal currents are found in the SoG in agreement with observations (Candela et al., 1990) and local tidal models (e.g. Tejedor et al., 1998, 1999; Sannino et al., 2004). West of the SoG there is an interesting transitional pattern between the NA/GoC and the SoG tidal regimes, with a strong decrease in tidal current amplitude and a veering in the orientation of the tidal current ellipses.

In the GoC the wavy pattern of the current ellipses field is easily noticeable. This interesting feature has been first noticed by Quaresma and Pichon (2013) using a regional (32.0° to 46.0°N and from 16.0° to 1.0°W) barotropic version of HYCOM (Bleck, 2002). They interpret these wave-like structures as a consequence of along-shelf tidal wave modulation by evenly spaced bathymetry features.

The interaction of the barotropic tide with these bottom topography features leads to the generation of internal tides. Müller et al. (2012) demonstrated using a 0.1° resolution MPIOM configuration (STORMTIDE) that with the inclusion of tidal forcing in a global OGCM the model was capable of simulating mode-1 internal tides in the World Ocean. Li et al. (2015) showed that this holds also for mode-2 internal tides, with a shorter wave-length of 45–80 km.

Camarinal Sill, the main sill of the SoG, represents one of the most

**Table 2**
List of numerical experiments.

| Experiment | Start fields | Length | SoG | Tidal forcing |
|---|---|---|---|---|
| TIDE | CLIM | 13 years | open | on |
| NOTIDE | CLIM | 13 years | open | off |
| LATE_SPINUP | TIDE YEAR 13 | 1 year | closed | on |
| FWS_TIDE | END OF LATE_SPINUP | 8 years | closed, with prescribed MOW source | on |
| FWS_NOTIDE | END OF LATE_SPINUP | 8 years | closed, with prescribed MOW source | off |
| NWS_TIDE | END OF LATE_SPINUP | 13 months | closed | on |
| NWS_NOTIDE | END OF LATE_SPINUP | 13 months | closed | off |

**Fig. 3.** M$_2$ cotidal chart from a) MPIOM-SPAN10, and b) HAMTIDE data-assimilative model (Taguchi et al., 2014). Greenwich phases are plotted every 30°, colorbar indicates tidal amplitudes in m.

extreme examples of internal tide generation (e.g. Morozov et al., 2002). These oscillations are more evident at the transition layer between the Atlantic and Mediterranean waters, which is often identified with an isohaline between 37.0 and 37.5 psu (Bray et al., 1990, 1995; Bryden et al., 1994). A Hovmøller diagram of model salinity (Fig. 7) at Camarinal Sill shows that the model places the mean interface (contoured lines show 37.0 (white) and 37.5 (black) isohalines) around 120 m depth (e.g. Bray et al., 1990, 1995; Sannino et al., 2002) and reproduces the spring-neap cycle and diurnal inequality of the large tidal vertical oscillations of the Atlantic-Mediterranean interface. The modelled mean depths and standard deviations of the 37.0 and 37.5 isohalines at Camarinal sill are 106 ± 27 m and 130 ± 30 m, respectively. These results are in good agreement with those obtained from previous modelling studies (e. g. Wang, 1993; Izquierdo et al., 2001; Sannino et al., 2004; Vlasenko et al., 2009;

Sánchez-Garrido et al., 2011) and observational campaigns. For comparison, Bray et al. (1990) identified the Atlantic-Mediterranean interface with the 37.5 psu isohaline on the basis of observational data from the Gibraltar Experiment 1985–1986 (Kinder and Bryden, 1987). At Camarinal sill they reported a mean interface depth of around 120 m with M$_2$ oscillation amplitudes ranging from 30 to 50 m (increasing from north to south). Using the same data set Bryden et al. (1994) chose the 37.0 psu isohaline as the interface at Camarinal Sill and found that it oscillated vertically with a standard deviation value of 47 m. Bray et al. (1995) placed the mean interface depth at Camarinal Sill between 100 and 125 m, corresponding to the 37.2 psu isohaline, using five cross strait hydrographic sections repeated several times and also belonging to the Gibraltar Experiment 1985–1986. This comparison shows that the model simulates properly the internal tide in the SoG, however the horizontal resolution is too poor to generate the existing
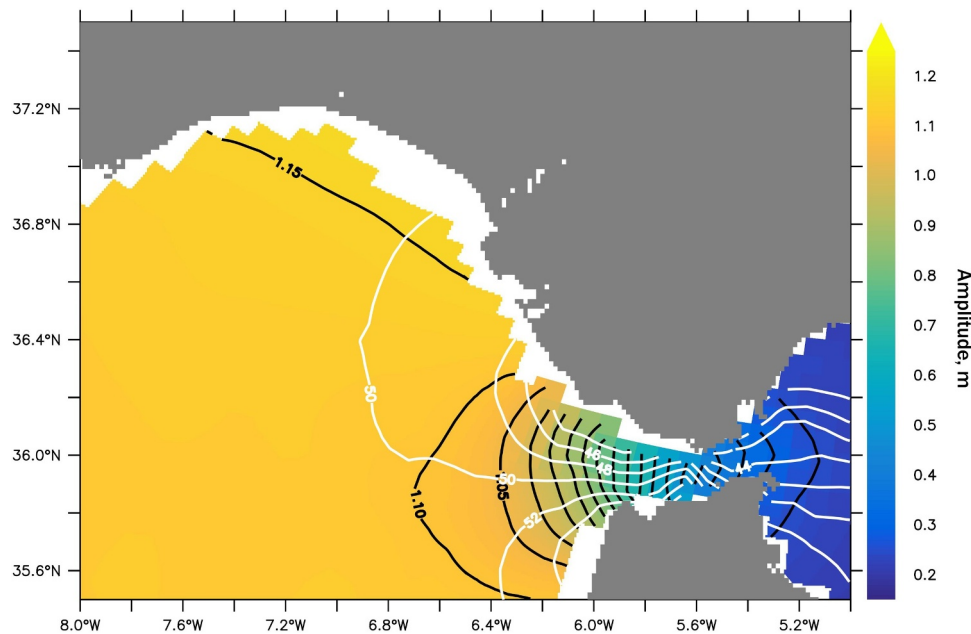
**Fig. 4.** Detailed $M_2$ cotidal chart from MPIOM-SPAN10. Greenwich phases are plotted every 2° with white isolines, colorbar and black isolines indicate tidal amplitudes in m.

short-period large amplitude internal waves.

MPIOM-SPAN10 also reproduces the existence of internal tides in the GoC, generated mostly at Gorringe Bank and S. Vicente Spur (Fig. 8), in full agreement with the location of 'hotspots' for the generation of the $M_2$ internal tide reported by Quaresma and Pichon (2013).

*3.3. Effect of tides on the ocean climate in the GoC*

Fig. 9 shows five salinity sections from East to West across the SoG and GoC as indicated in Fig. 2. Displayed is the annual mean salinity of the last year of experiment TIDE. At the eastern side of the SoG (Fig. 9a) the Atlantic-Mediterranean interface is placed at the correct depth, shallower at the North due to Coriolis acceleration in agreement with observations (e.g. Bryden et al., 1994, Bray et al., 1995). To the west, the Mediterranean outflow becomes less salty due to mixing and entrainment with ambient waters, and sinks gradually to an equilibrium depth of 1100 m at C. Santa Maria, first as a bottom current and finally as a slope-bounded undercurrent: The Mediterranean Undercurrent, which turns north after passing the Cape of S. Vicente. The results from experiment TIDE on both MOW location and properties in the SoG and the GoC are in good agreement with the climatological data from the World Ocean Data base (Supp. Mat. Fig. S1a), and with previously published salinity sections in the eastern GoC (Ochoa and Bray, 1991; Baringer and Price, 1997). In contrast, results from experiment NOTIDE show clear differences to climatological data already in the eastern GoC (Section c in Supp. Mat. Fig. S1b). The differences increase substantially towards the west. A similar behaviour is observed for temperatures (Fig. S2).

Direct comparison of the results from experiments TIDE and NOTIDE reveals the effect of tides. Figs. 10a and b show the salinity field at approximately the MOW depth (1143 m) for both experiments in year 13. Starting from the same initial conditions both experiments reproduce the MOW salinity anomaly in the eastern NA. Both experiments show a finer structure than the lower resolution (0.25°) climatology (Fig. 10c) and somewhat higher salinities in the western periphery off the Iberian Peninsula.

However, while the fields from experiment TIDE better resemble the climatological salinity distribution, experiment NOTIDE shows a too

salty tongue from the GoC to the southwest (Fig. 10b), which is at odds with the pathways of MOW spreading derived from observations or climatological data analysis (e.g. Zenk and Armi, 1990; Daniault et al., 1994; Iorga & Lozier, 1999a; Bower et al., 2002; Carracedo et al., 2014, see also our scheme in Fig. 1). Baringer and Price (1997) and Iorga and Lozier (1999) used the 36.25 psu isohaline as the minimum limit for defining the MOW outflow in the GoC and estimated the maximum width of the MOW plume as 65 and 50 km, respectively, in very good agreement with experiment TIDE result (Fig. 10, black isohaline).

The origin of this excessive southward salt flux in experiment NOTIDE is related to a gradual increase in the salinity of the GoC at MOW depths. During the course of the simulation, the GoC becomes saltier, and the salinity surplus propagates southwestward, as a mid-depth salinity front. A meridional cross-section through the GoC at 8° W (Fig. 11) further illustrates the differences between the TIDE (Fig. 11a) and NOTIDE (Fig. 11b) experiments in this area: in both runs the MOW core depth of 1100 m is slightly too shallow compared to observations (Fig. 11c) and the double salinity core is not reproduced. These are caveats common to other MOW simulations (e.g. Treguier et al., 2003; Jia et al., 2007) and in our case they are likely related to an excessive entrainment favoured by the staircase topography (Treguier et al., 2003). Papadakis et al. (2003) demonstrated that a shallower Mediterranean undercurrent produces higher meddy activity and Artale et al. (2003) concluded that the vertical position of MW could have an impact on the structure of AMOC. However Ivanovic et al. (2013) showed that for a proper AMOC simulation it is necessary to attain a MOW plume centered at 1000 m. As long as the MOW depth is similar in both experiments and around 1100 m this misrepresentation will have no impact on our evaluation of the role of tides in MOW spreading.

Remarkably, in experiment NOTIDE the MOW plume is not a wall-bounded gravity current spreading along the Iberian continental slope but rather a mid-depth salinity anomaly extending to the south of the GoC (Fig. 11b). This striking difference between the experiments in the pattern of MOW spreading into the NA is fully attributable to the inclusion of the tidal potential in the TIDE control experiment. Temperature sections (Fig. S3) reproduce the same patterns as salinity.

There are two potential non-exclusive causes for this effect of tides on the ocean climate in the GoC: The first and well known cause is that
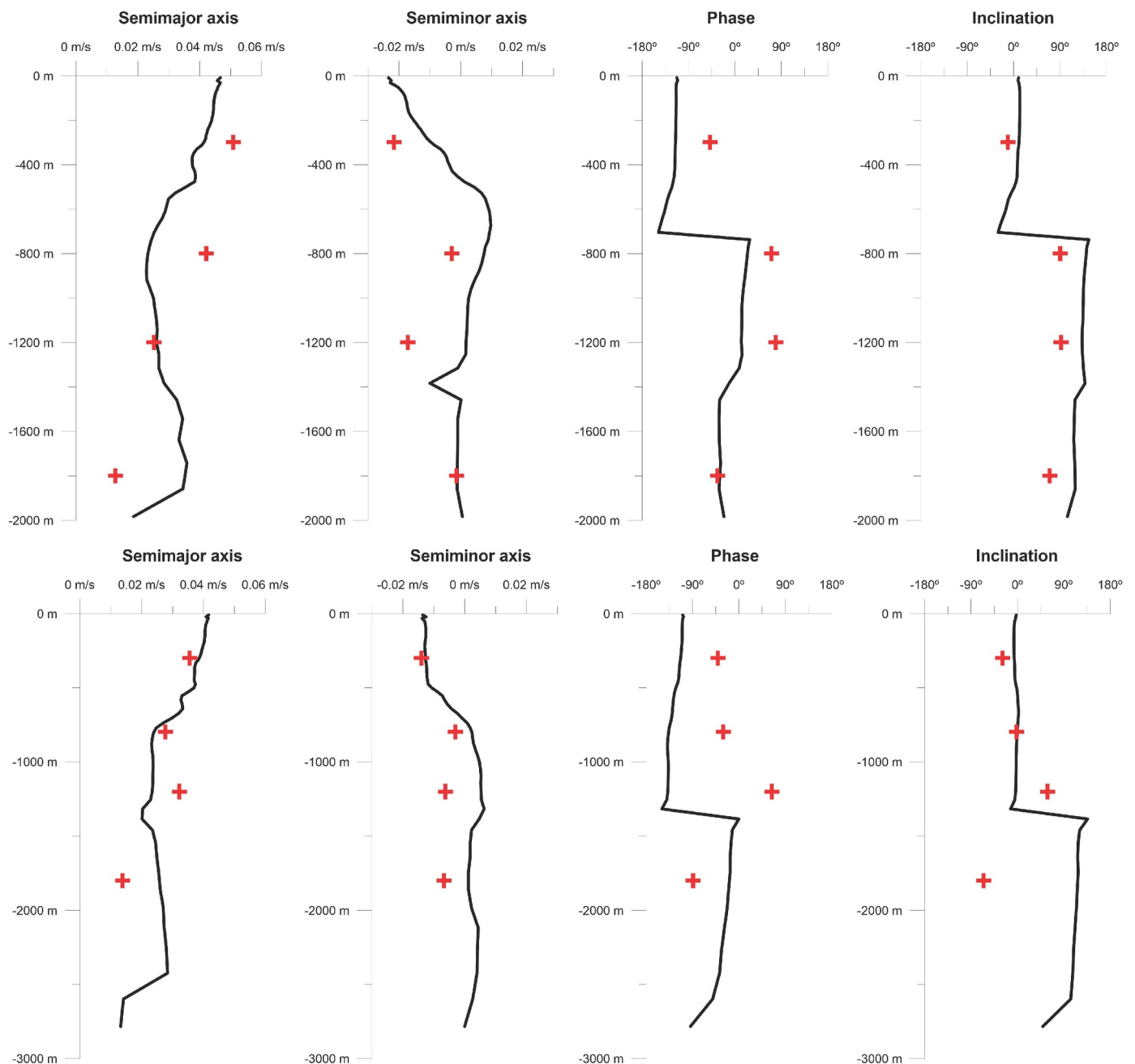
**Fig. 5.** Profile of observed (red crosses) and modelled (black line) M$_2$ tidal current ellipse parameters at the two mooring sites (see Fig. 6) in the GoC.

tides have a strong effect both on the properties and on the amount of MOW exiting the SoG, due to the intense tidal mixing and the correlation between horizontal tidal currents and interface vertical excursions (see Fig. 7). Apparently, the effect of tidally induced mixing in the SoG on MOW properties was first proposed by Seidler (1968), and has been studied in several papers and shown to be of considerable importance. Bryden et al. (1994) report an important contribution of tidal fluctuations at the SoG to the mean exchange flows, which has an estimated mean value in the range from 0.67 to 1.78 Sv (Bryden et al., 1994).

In our experiments the inclusion of tides produces an increase in the mean water exchange at Camarinal Sill section (SoG) from 0.9 Sv (NOTIDE) to 1.5 Sv (TIDE) and a decrease of the salt transport to the GoC from 1.21 psu Sv (NOTIDE) to 1.10 psu Sv (TIDE) (Table 3). This result agrees with the modelling study of Sannino et al. (2004), who found that the effect of the semidiurnal tide is to increment the mean

transport by about 30%.

The second potential cause for the differences between the two experiments is the effect of tides on the spreading of the MOW within the GoC. Indeed, there are clear differences in the time mean velocity fields at 1143 m depth between the TIDE and NOTIDE experiments (Fig. 12) that are consistent with the respective salinity distribution shown in Fig. 10. Experiment TIDE (Fig. 12a) presents an open cyclonic circulation with westward currents at the Iberian slope and increasing velocities between Cape S. Vicente and Gorringe Bank, guaranteeing an efficient export of MOW to the Tagus abyssal plain mostly through the gap between S. Vicente Spur and Gorringe Bank. Bower et al. (2002) estimated mean velocities between 0.1–0.2 m s$^{-1}$ in this area on the basis of RAFOS floats. Similar values have been reported by Barbosa et al. (2015) from ADCP measurements taken during SEMANE2000 campaing (Section 04 at 8°44′W). Further, the MOW core meanders west and northwest propagating the themohaline anomaly at
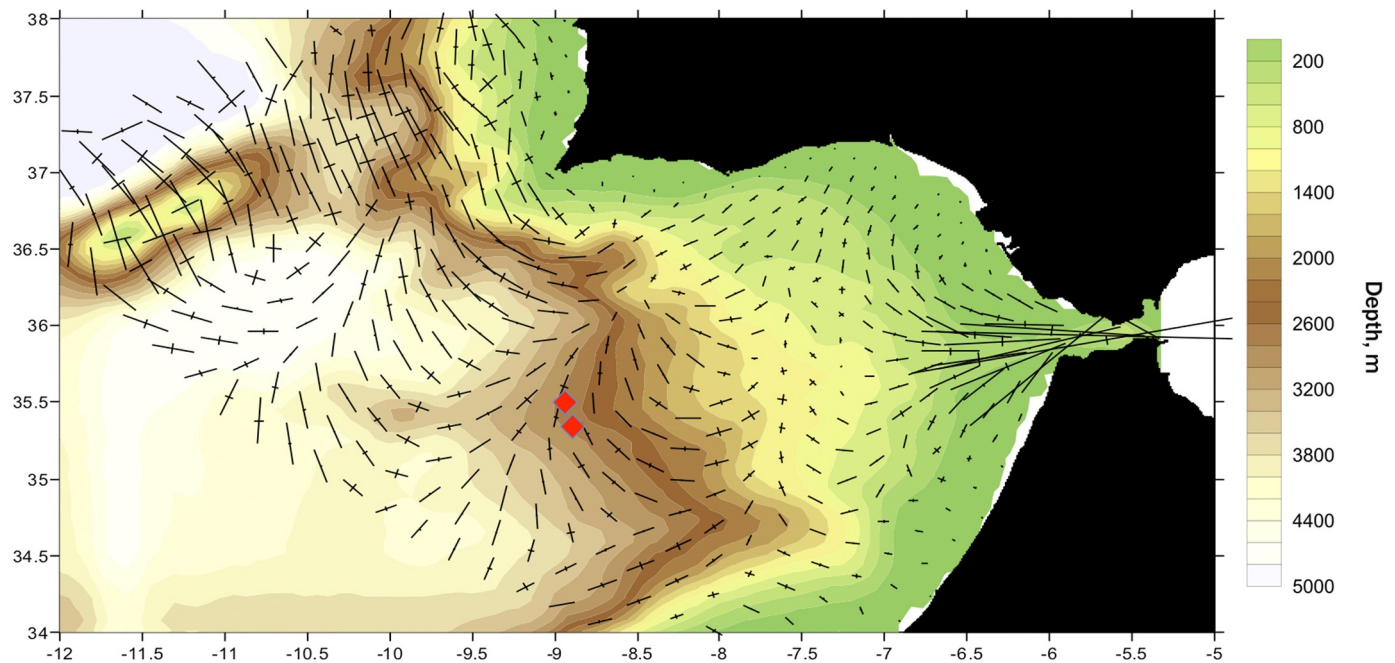
**Fig. 6.** Depth-averaged modelled M₂ tide current ellipses. Red diamonds indicate the locations of the current meters used in Fig. 5. Color shading represents depth.
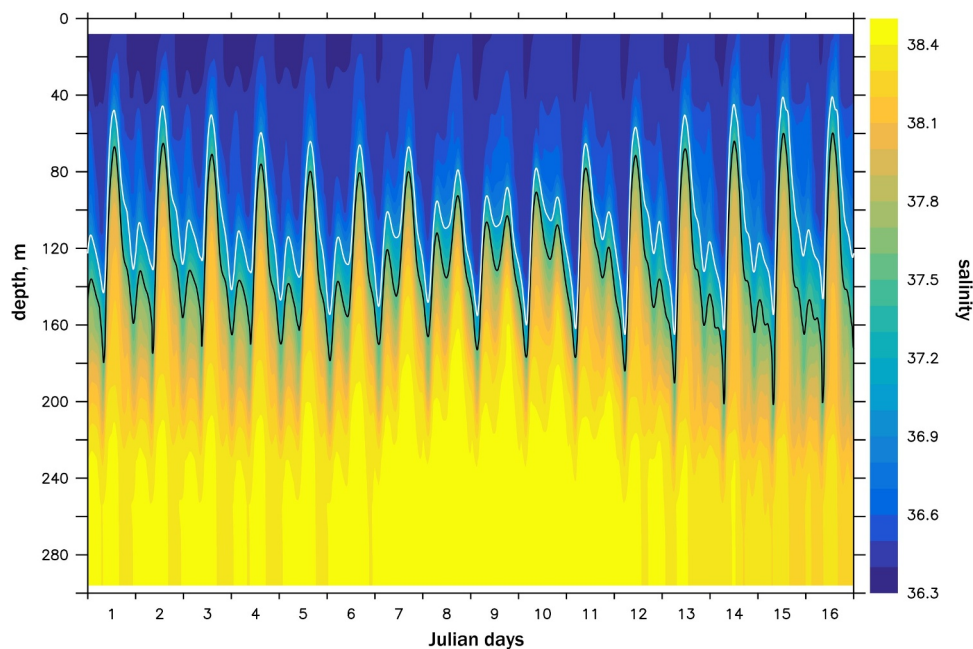


**Fig. 7.** TIDE time series of salinity along a spring-neap tidal cycle (15 days) at a grid point located at Camarinal sill in the SoG. Contours represent the 37.0 (white) and 37.5 (black) isohalines.

intermediate depths. Along the African slope the flow is mostly poleward supplying fresher Antarctic Intermediate Water (AAIW, Barton, 1989; Machín and Pelegrí, 2009). This circulation pattern is close to the classical view (e.g. Zenk and Armi, 1990; Daniault et al., 1994; Iorga and Lozier, 1999b) that has been confirmed by more recent studies (e.g. Carracedo et al., 2014).

The NOTIDE (Fig. 12b) experiment depicts a very different velocity field, with much less small-scale structure and a dominant southwestward flow, which is in disagreement with all observational and climatological evidence. There is a clear correspondence between the velocity and the salinity fields in both experiments and it is evident that the TIDE solution is much better than the NOTIDE one. However, it is not obvious what ruins the NOTIDE solution: Does the difference in

water and salt exchanges through the SoG drive the circulation changes in the GoC, or do tidally induced differences in the GoC circulation generate a different MOW spreading pattern?

In the remainder of this paper we will address this question by performing a set of additional experiments, where we exclude the effect of changes in amount and properties of MOW transport through the SoG.

### 3.4. Closed-strait fixed water source experiments

The difference between experiments TIDE and NOTIDE shows the effect of tides both in the SoG as well as in the GoC. To be able to isolate the effect of tides in the GoC a new set of experiments was carried out
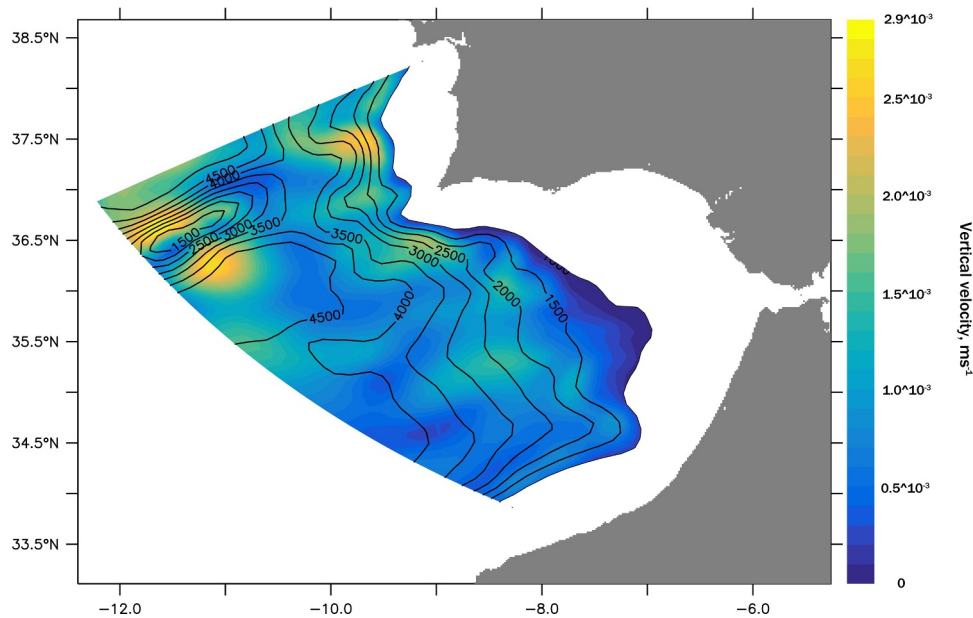
**Fig. 8.** Amplitude of the $M_2$ vertical velocity component (color scale, ms$^{-1}$) at 1143 m depth from experiment TIDE. Contour lines show isobaths (m).

with a closed SoG and a fixed water source (FWS): A continuous water source (0.8 Sv, 38.5 psu, 13 °C) was placed at the bottom of the first cell (354 m depth) in the Atlantic side of the SoG. In order to easier trace the spreading of the FWS water a passive tracer was included in these simulations, marking the prescribed MOW source water. This setup guarantees that we have identical salt, water and tracer flow into the GoC for the FWS_TIDE and FWS_NOTIDE experiments and that the only differences between these two experiments are due to tidally induced effects outside the SoG, especially in the GoC. The bathymetry file was modified to artificially close the SoG.

As spin up, the closed strait model configuration was run for 1 year without prescribed source of MOW starting from year 13 of experiment TIDE. This procedure removed the MOW from the GoC. Starting from this second spin up state two experiments were integrated for 8 years with prescribed FWS with (FWS_TIDE) and without tidal forcing (FWS_NOTIDE). Following we present results averaged over the last year of the FWS experiments. The FWS experiments show the same MOW spreading pattern as those with an open SoG (baseline): while the source water tracer field in the FWS_TIDE experiment (Fig. 13a) reproduces the accepted MOW spreading pathways (Fig. 1), the results from experiment FWS_NOTIDE (Fig. 13b) indicate a clearly unrealistic southward salt flux. The GoC gets gradually saltier at mid-depths, and the salinity excess propagates to the southwest. The correspondence between the FWS tracer fields and the baseline salinity fields (Fig. 10) is more than evident. The results from the two FWS experiments clearly indicate that the modification of the mean water exchange flows by intense tidal mixing and tidal rectification in the SoG is not decisive for the changes in the MOW spreading pattern between the TIDE and NOTIDE experiments.

Moreover, differences in tracer fields from FWS_TIDE and FWS_NOTIDE (Fig. 13) are closely related to changes in the circulation pattern within the GoC (Fig. 14). The velocity fields in experiments FWS_TIDE and FWS_NOTIDE to a large extent mimic those of the TIDE and NOTIDE baseline experiments, resulting, in the tidal cases, in a further westward transport of MOW along the Iberian slope. This demonstrates that tidally induced processes within the GoC are causing the differences in the spreading of MOW in the GoC between experiments TIDE and NOTIDE. Additionally, the time evolution of the source water plume in FWS_TIDE and FWS_NOTIDE (see Animation 1 in Supp. Mat.) is closely linked to the velocity fields and shows differences already at initial stages, when it is too early for changes in density field to

cause a substantial impact on the dynamics. NOTIDE experiments with increased values of vertical eddy viscosity and diffusivity show an impact on MOW vertical structure, but do not change the preference for a southwestward spreading. This points toward tidally induced circulation changes as cause of the difference in advective tracer transport. The prime suspect is tidally induced residual current. In the following Section we will investigate this mechanism.

### 3.5. Tidally induced residual currents in the GoC: the advective transport mechanism

In order to test the hypothesis that the changes in the spreading of MOW due to inclusion of tides are dominated by advection through the tidally induced residual currents, we determined the residual currents from two short additional sensitivity experiments. We run the closed SoG SPAN10 configuration without any water source (no water source experiments, NWS) with and without tidal forcing. Experiments were started from the same spin up as FWS experiments, and then the model was run for 13 months with and without tidal forcing without any water source (NWS_TIDE and NWS_NOTIDE).

From the last 12 months of these experiments we calculated the tidal residual velocity and sea surface height (SSH) fields. Fig. 15 shows the depth-integrated tidal residual velocity between the sea surface and 1858 m depth and tidal residual SSH in the GoC. The modelled tidal residual velocity field is closely related to the contours of tidal residual SSH, which in turn are linked to bottom topography (see Fig. 16a). The tidal residual SSH field is characterized by two depressions (right south of Cape S. Vicente and east of Gorringe Bank, see d1 and d2 in Fig. 16a) each associated with a corresponding depth-integrated cyclonic residual circulation in the upper 1858 m (Fig. 15). The largest tidal residual currents at 1143 m depth, up to 3 cm s$^{-1}$, are located at the slopes of Gorringe Bank (GB) and around S. Vicente Spur (SVS) west of Portimao Valley (see Fig. 2 or Fig. 16a for locations). Thus, these tidally-induced residual currents might be responsible for the differences in MOW spreading in the TIDE and NOTIDE control experiments: They provide a more efficient advective export of MOW to the NA from the GoC in the TIDE experiment. Conversely, the lack of this tidal residual transport causes an accumulation of MOW in the GoC, which results in gradually increasing salinity at mid-depths. Ultimately this salinity anomaly will propagate as a salinity front to the southwest following the North African slope.
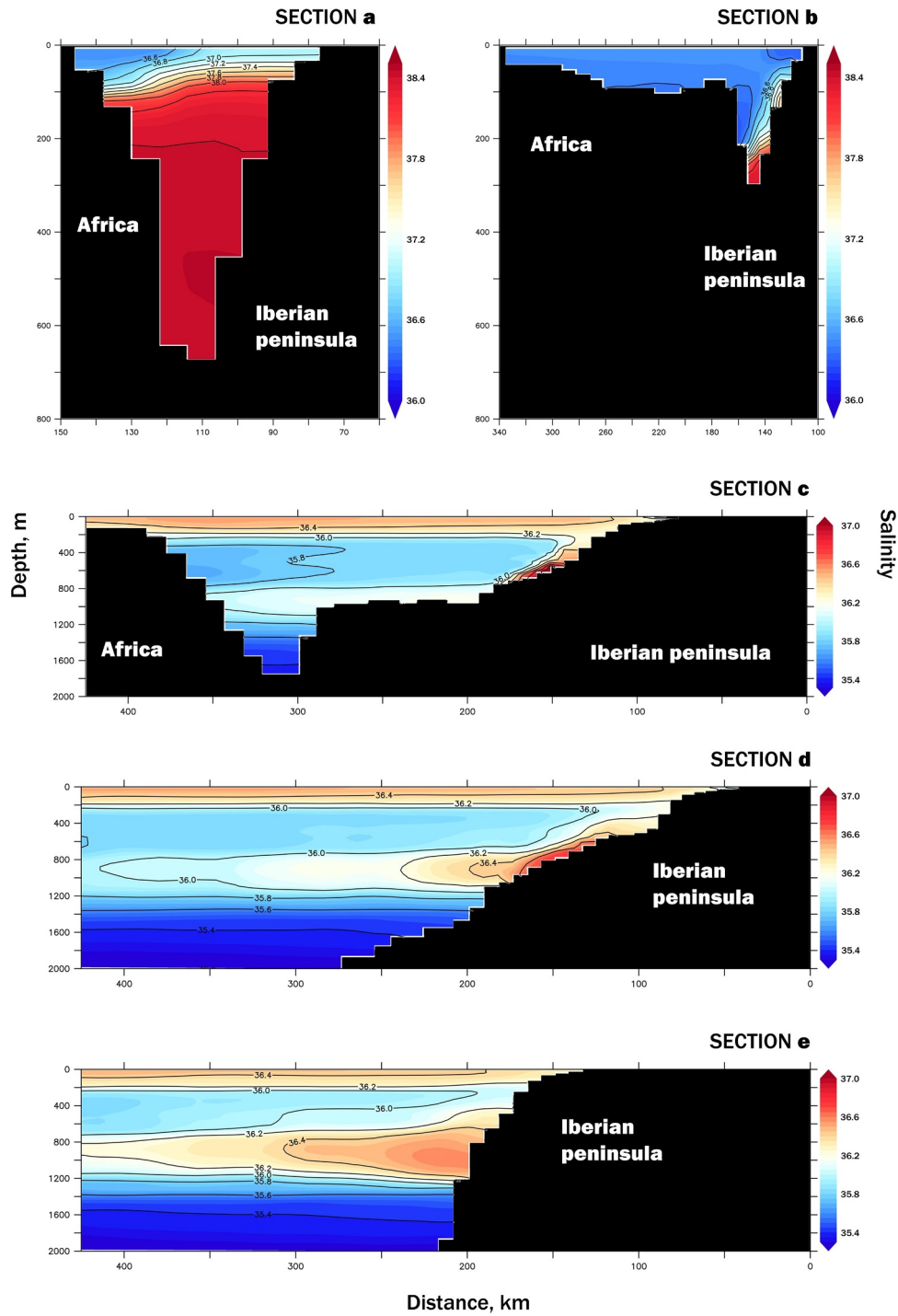
**Fig. 9.** TIDE salinity cross-sections (see black lines in Fig. 2).

To check the validity of the proposed mechanism as initial trigger we used the high-frequency (3456 s) output of the first 2 years of FWS_TIDE and FWS_NOTIDE (the fixed water source as 0.8 Sv, 38.5 psu, 13 °C, [Tracer] = 1.0) to calculate offline the advective tracer transport, $F_{Ti}$, across northwestern and southwestern boundaries enclosing the GoC (Fig. 16a).

$$F_{Ti} = \int_0^L \int_{-h}^{\zeta} \mathbf{v_i} \cdot Tr_i \, dz ds \qquad \begin{cases} i = T; \ FWS\_TIDE \\ i = NT; \ FWS\_NOTIDE \end{cases} \tag{1}$$

where $\mathbf{v_i}$ and $Tr_i$ are velocity and tracer concentration, $L$ is the length of the boundary, and $h$ and $\zeta$ are the local depth and free surface elevation, respectively.

The "zonal" (across the solid line, i.e. between Gorringe bank (GB) and S. Vicente Spur (SVS)) and "meridional" (dotted line) tracer transports (Fig. 16a) show clear differences between the FWS_TIDE (black line) and FWS_NOTIDE (red line) runs, with the FWS_TIDE tracer exiting the GoC mainly through the GB-SVS section (positive values indicate fluxes out from the GoC) as reported from observations. Bower et al. (2002) report that most of the AMUSE floats (60%) exited the GoC through the GB-SVS section. Over the two years presented, the evolution of the advective tracer transports shows a clear seasonality, indicative of the importance of the atmospheric forcing in the GoC circulation at depth (Carracedo et al., 2014). Tracer export from the GoC is more efficient in the FWS_TIDE case, being always larger across
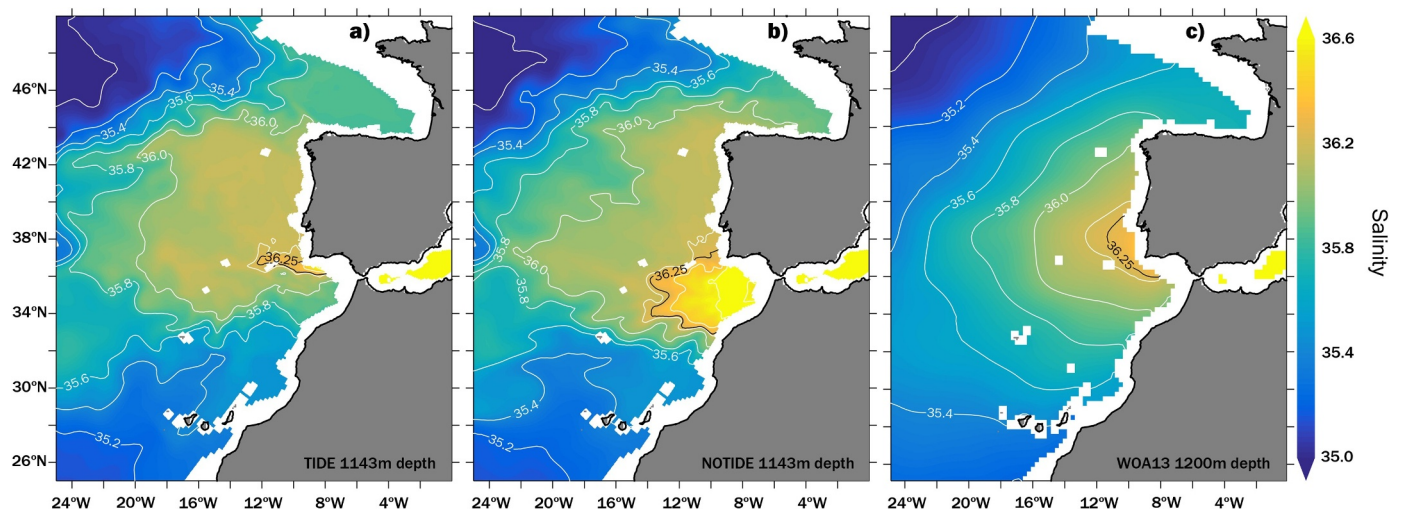
**Fig. 10.** Salinity fields at 1143 m depth. a) TIDE, b) NOTIDE, and c) WOA13 (Zweng et al., 2013).

the northwestern boundary than across the southwestern. Conversely, FWS_NOTIDE tracer transport is larger across the southwestern boundary, and very small across the western boundary, indicative of artificial southwestward spreading of MOW in the GoC. Eventually, FWS_NOTIDE simulates negative tracer transport across the GB-SVS section, pointing to a recirculation of MOW exiting through the southwestern boundary. The radical difference in MOW spreading pathways from the GoC is readily seen in Fig. 17, showing the FWS_TIDE - FWS_NOTIDE difference in tracer concentration (averaged over year 2) along de GoC box boundaries.

We have also recalculated the FWS_NOTIDE tracer transport adding the constant 3D tidal residual velocity field obtained from the NWS experiments ($\boldsymbol{v_{res}}$) to the time-varying FWS_NOTIDE velocity ($\boldsymbol{v_{NT}}$) (Fig. 13b,c, grey lines) and using the FWS_NOTIDE tracer fields ($Tr_{NT}$) according to Eq. (2)

$$F_{Tr} = \int_0^L \int_{-h}^{\zeta} (\boldsymbol{v_{res}} + \boldsymbol{v_{NT}}) \cdot Tr_{NT} \, dzds \qquad (2)$$

The result approaches the transport calculated from FWS_TIDE, with a preferred pathway between GB and SVS. This convergence is more evident after the first year, when the tracer concentration along the boundaries is larger. This confirms that advection with the tidal residual currents is the main contributor to the observed differences in MOW spreading in the GoC between our tidal and no tidal experiments.

The FWS experiments were repeated for different source water properties (denser and lighter source waters), different water source production rates (from 0.5 Sv to 1.2 Sv) and with varying viscosity, diffusion and bottom friction coefficients. In all tested cases the results remain at large unchanged: when tidal forcing is not present, the GoC gets extremely saltier at mid-depths and MOW flows in excess to the southwest along the North African shelf slope. This unrealistic behaviour is corrected when tidal forcing is included. This set of additional experiments (not shown) confirmed our hypothesis that the difference in the spreading of MOW in the GoC in experiments TIDE and NOTIDE is essentially determined by tidally induced processes in the GoC.

## 4. Discussion

The strong effect of tides on the exchange through the SoG by enhanced mixing and tidal rectification has been widely recognized. Recently, Sannino et al. (2015) investigated the role of tides in the Mediterranean thermohaline circulation by means of a pair (tide/no tide) of numerical experiments with an eddy resolving MITgcm configuration. The results suggest that the inclusion of explicit tidal forcing in an eddy resolving Mediterranean model has non negligible effects on

the simulated circulation, besides the intensification of local mixing processes. However, the influence of tides on the spreading of MOW in the GoC has been much disregarded, despite the fact that MOW flows as a narrow slope undercurrent in the mesotidal GoC, where the continental shelf and slope change abruptly direction and present marked bathymetric irregularities which can trigger strong nonlinear interactions. On the other hand, the importance of topography interaction and mixing on the MOW plume adjustment in the GoC (e. g. Price and Baringer, 1994; Peliz et al., 2007; Sánchez el al. 2017) is well established.

The inclusion of tides obviously improves the simulated spreading of MOW in the GoC and the NA. Advection by the residual currents contributes to this improvement, as our FWS sensitivity experiments clearly demonstrate. Tidal impact on mean circulation has been observed at a basin scale in other MPIOM configurations (Sein et al., 2015; Weber and Thomas, 2017). Using a pure barotropic model Quaresma and Pichon (2013) also identified Gorringe Bank and S. Vicente Spur as the locations with larger $M_2$ tidal residual currents in the GoC. Their residual currents are smaller than those we present here, however it is known that in case of stratification tidal rectification and tidal mixing intensify the residual currents (Maas and Zimmerman, 1989; Chen et al., 1995). Indeed, recent studies report the existence of tidal residual currents of significant magnitude. Kurapov et al. (2010), in a process study with the Regional Ocean Modelling System (ROMS), demonstrated that moderate internal tides (horizontal velocities $O$ ($10^{-1}$ ms$^{-1}$)) can induce differences in the subinertial velocity field of the same order of magnitude through the changes in the bottom boundary layer variability, resulting in a larger bottom stress and divergence in the Reynolds stresses associated with the baroclinic tidal flow. More recently Musgrave et al. (2017) reported the generation of time mean flows by tides of up to 0.15 ms$^{-1}$ in some regions of the Mendocino Ridge with complex topography, and even hypothesized that such tidally-induced circulations may play a role in the lateral spreading of water masses from the ridge crest into the ocean's interior.

The unrealistic southwestward spreading of MOW in the GoC and in the NA found in the NOTIDE experiments is a problem found in several global or basin-scale models without tides. Jia et al. (2007) investigated an explicit Mediterranean-Atlantic exchange through a wide-open SoG in the global OCCAM model. They focused on the behaviour of MOW in the NA and, remarkably, their bias pattern of the salinity field at MOW depths closely resembles that of our NOTIDE experiment, with salinities as high as 36.5 g/kg at 30°N off the North African coast (their Fig. 10a). Gary et al. (2011) also observed a similar anomalous presence of Mediterranean waters between 25°N and 40°N in the eastern Atlantic in the 1/12° FLAME output. According to our results it starts with a less
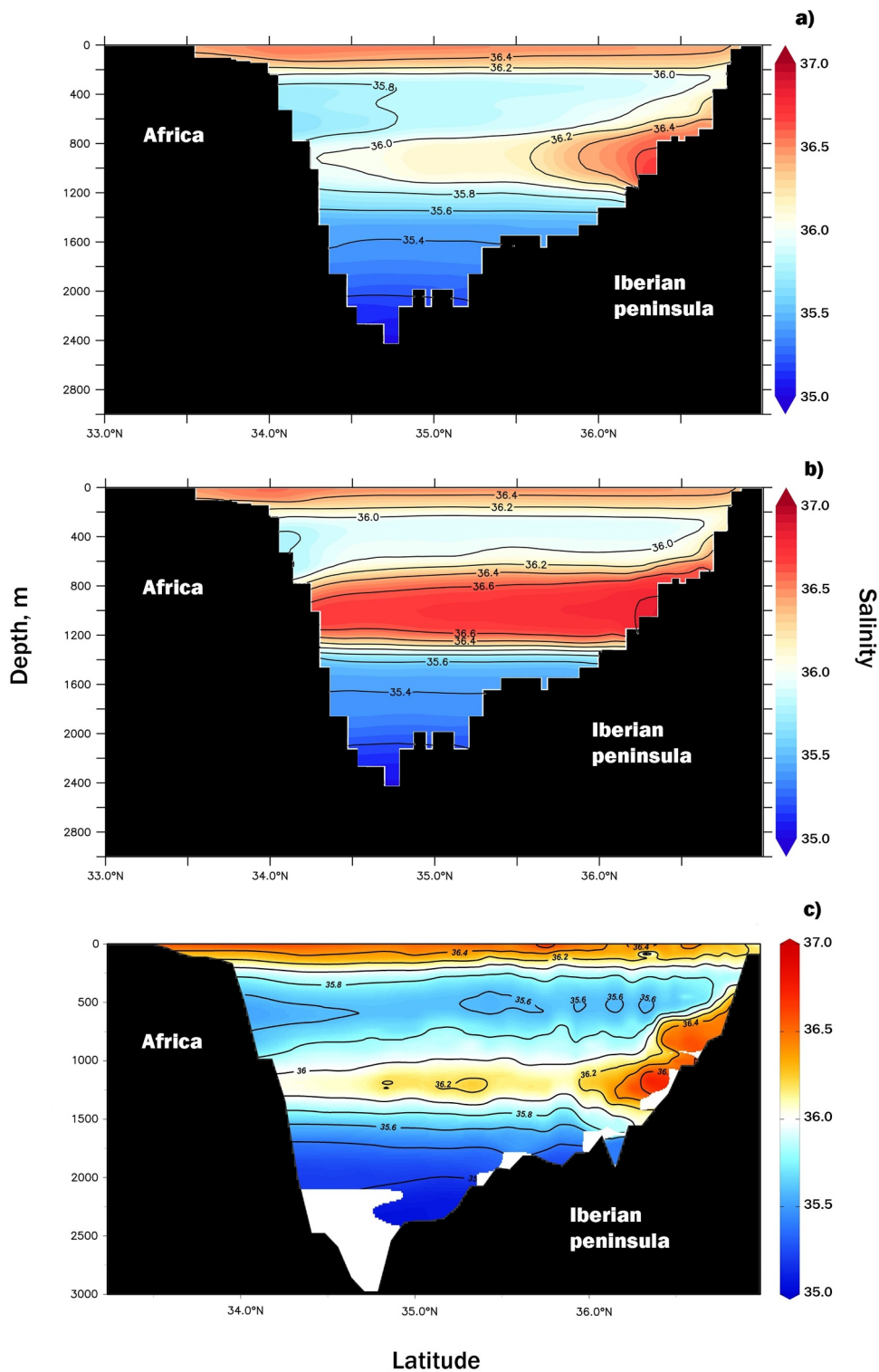
**Fig. 11.** Salinity sections across the GoC at 8°W. a) TIDE, b) NOTIDE, and c) observations from World Ocean Database (Boyer et al., 2013).

**Table 3**
Exchange through the SoG. In and out prefixes indicate westward and eastward directions, respectively. $\bar{S}_{in}$ and $\bar{S}_{out}$ are inflow and outflow mean salinity.

|  | Inflow (Sv) | Outflow (Sv) | Netflow (Sv) | Salt influx (psu Sv) | Salt outflux (psu Sv) | Net salt transport (psu Sv) | $\bar{S}_{in}$ | $\bar{S}_{out}$ |
|---|---|---|---|---|---|---|---|---|
| Tide | 1.525 | −1.520 | 0.004 | 56.24 | −57.54 | −1.10 | 36.87 | 37.86 |
| Notide | 0.874 | −0.861 | 0.013 | 31.85 | −33.06 | −1.21 | 36.55 | 38.44 |
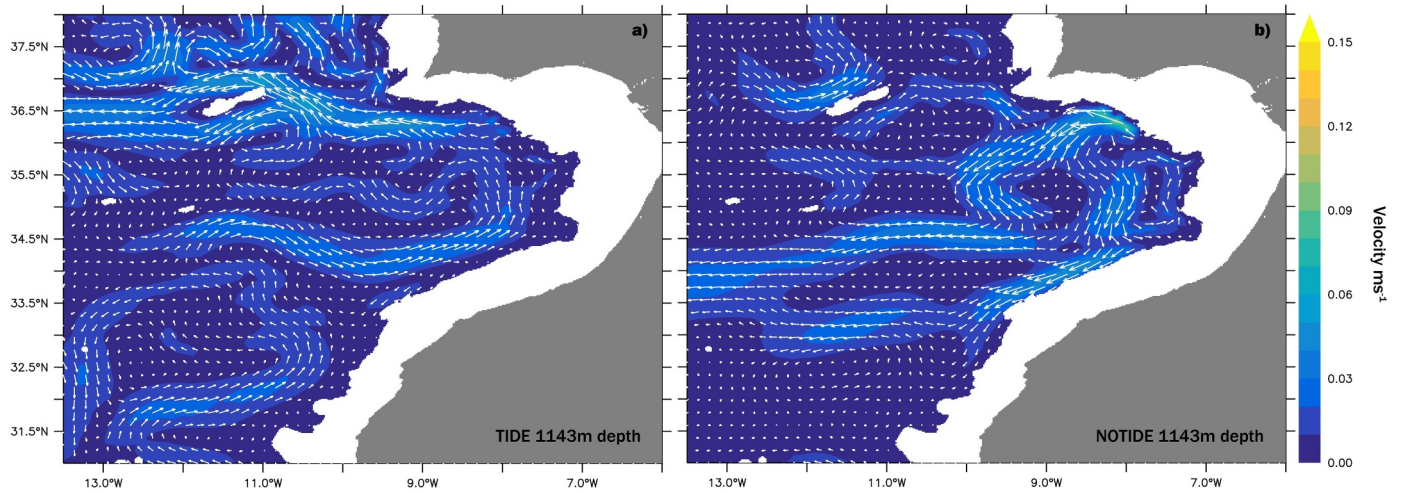
**Fig. 12.** Horizontal velocity field at 1143 m depth. a) TIDE, b) NOTIDE.

efficient evacuation of MOW through the western boundary of the GoC. This produces a MOW accumulation with a subsequent southwestward spreading along the North African coast, which finally triggers the collapse of a poleward fresher flow along the African coast (Barton, 1989) and blocks the northward penetration of AAIW (whose core is slightly shallower). The importance of an adequate supply of fresher AAIW for a proper Mediterranean Water formation at the GoC is supported by the analysis of hydrographic data provided by Iorga and Lozier (1999a,b), by the cluster analysis data presented by Machín and Pelegrí (2009) and by the climatologically-based study of Carracedo et al. (2014). Cutting the freshwater supply that would entrain underlying salty MOW at the GoC (Iorga and Lozier, 1999a,b) leads to an additional gradual salinification in the GoC and a disruption of the water mass structure and circulation in the eastern boundary NA.

However, limited area models have been able to properly simulate the spreading of MOW along the SW Iberian margin while simulating a realistic water exchange through the SoG without accounting for tides (e.g. Papadakis et al., 2003; Drillet et al., 2005; Serra et al., 2005, 2010; Peliz et al., 2007, 2013; Xu et al., 2007; Bozec et al., 2011; Barbosa et al., 2015). This apparent contradiction seems to indicate that an appropriate choice of open boundaries conditions close to the Gulf of Cádiz and/or the use of variable horizontal mixing, bottom friction, relaxation or restoring can play a role similar to that of the explicit inclusion of tidal forcing in our experiments. This is compatible with the causal chain that according to our results leads to the degeneracy of the solution in the NOTIDE experiment: (1) less efficient MOW export through the western boundary of the GoC; (2) gradual increase of salinity in the GoC; (3) southwestward propagation of the salinity anomaly; (4) suppression of the poleward flow supplying fresher water to the GoC; (5) further salinity increase in the GoC. Limited area models offer a number of options to avoid any of the first three steps of this causal chain, among them prescribing/parameterizing the outflow through the SoG, reducing the MOW inflow into the GoC or enhancing the westward export of MOW (via varying bottom friction or horizontal
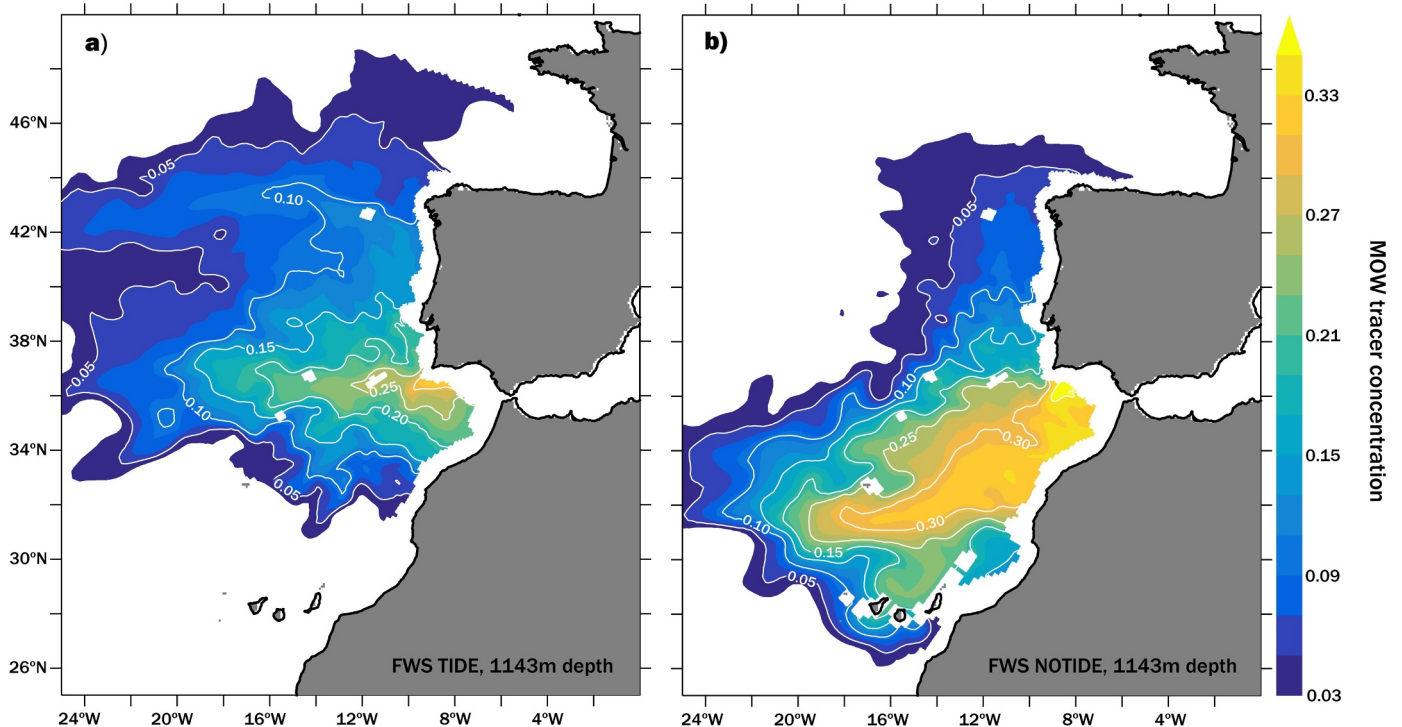


**Fig. 13.** MOW tracer concentration at 1143 m depth. a) FSW_TIDE and b) FWS_NOTIDE. .
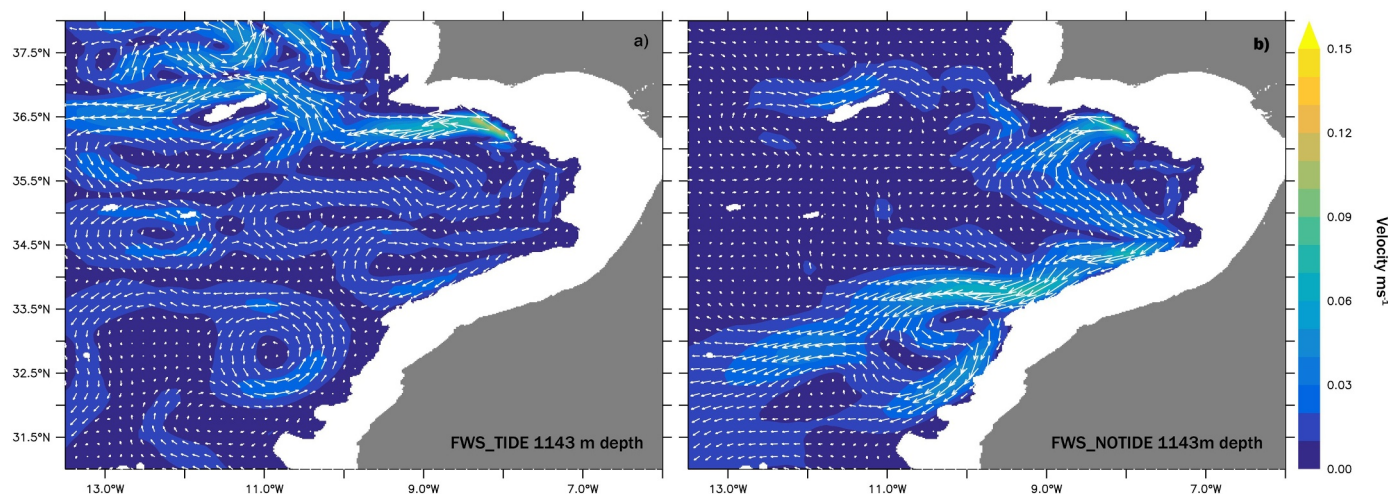
Fig. 14. Horizontal velocity field at 1143 m depth. a) FSW_TIDE and b) FWS_NOTIDE.

diffusivity), restoring salinity to climatology or by the open boundary conditions/sponge zones in the limited area models. Therefore limited area models can be successful without explicitly including tides.

Our results demonstrate that - in our model setup – the inclusion of explicit tidal forcing alone is able to correct the excessive southwestward spreading of MOW, reducing the biases in the northeast Atlantic. Using a global ocean model, we ensure that the model results in the GoC are not affected by information provided through the open boundary conditions. Tides may affect MOW spreading and properties through enhanced mixing or tidally induced residual currents. Indeed, mixing between the Mediterranean outflow and the Atlantic ambient waters takes place over a small distance, a few tens of km, and depends strongly on bottom topography (Price and Baringer, 1994; Jungclaus and Mellor, 2000). However, according to Quaresma and Pichon (2013) and to our modelling results, topography does not only have an influence on mixing, but also on the spatial structure of the tidal wave and the residual currents, which in turn might be originated by tidal mixing (e.g. Chen et al., 1995). This is evident in Fig. 6 where a pivotal point in the field of $M_2$ tidal current ellipse parameters is located in the Portimao Valley. This divergence in the orientation of the semimajor axes (Fig. 6) is also observed in tidal modelling results of Quaresma and Pichon (2013), where it is accompanied by a nearly 180° phase difference in maximum $M_2$ tidal velocities from west to east of the Portimao Valley. This is exactly the area with the largest values of the tidally induced residual current velocities, which closely follow the
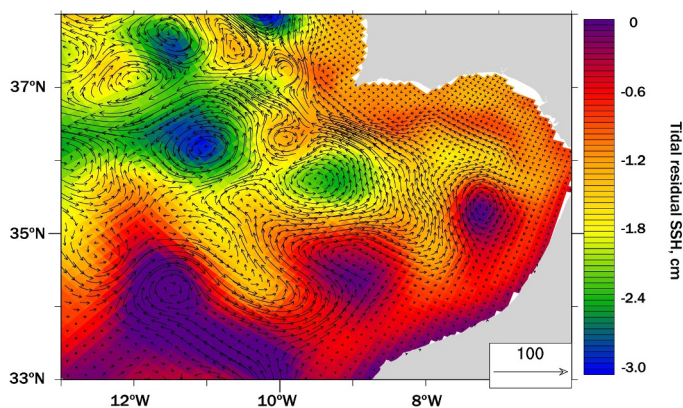


Fig. 15. Depth-integrated (from surface to 1858 m depth) tidal residual horizontal velocity (vector field, $m^2\,s^{-1}$) and SSH (shading, in cm). Both residual fields are calculated as the difference between 1-year averaged values from NWS_TIDE and NWS_NOTIDE.

sea surface height residual field (Fig. 15). The tracer transport calculations (Fig. 16) point out that the tidal residual currents play a lead role.

## 5. Summary and conclusions

MOW spreads as a basin-scale salinity anomaly at about 1000–1200 m depth through the NA forming the Mediterranean salinity tongue. After exiting from the SoG it transits as a narrow slope-bounded gravity plume the complex topography of the GoC. Therefore, small scale processes and local scale nonlinear interaction with tides and topography may have an impact on the MOW properties and its further spreading pattern in the NA.

To investigate the impact of tides on the MOW spreading it is necessary to take into account a wide range of spatial and temporal scales, which we have done by simultaneously resolving the local-scale processes at the SoG and the GoC and the larger-scale processes which may influence the NA climate, by means of using a highly zoomed setup of the global MPIOM with explicit simulation of tides.

The MPIOM simulation of the MOW is successful, in the sense that the depth and properties of the MOW core are properly reproduced after the 13 year long baseline experiments. While the experiment including tides resemble better the climatology and the established MOW spreading pathways, the experiment without tidal forcing simulates an excess of salinity at MOW depths in the GoC, which triggers a non realistic southward salt flux. This spreading of MOW along the African slope suppresses the supply of fresher AAIW by the poleward undercurrent on the eastern boundary. This feedback further enhances the salinity increase and the southwestward spreading of MOW. The resulting salinity bias pattern is common to some other global or basin scale models that do not include tides.

A series of process-study targeted numerical experiments was designed in order to reveal the mechanisms responsible for such differences in the MOW simulations with and without tides. From a detailed analysis of the experiments' high-frequency output we were able to conclude that the tidal residual currents, likely generated by the interaction of tides with local-scale topography, play a major role in the spreading of MOW in the GoC. According to our results tidal residual currents contribute to the advection of MOW west from the GoC, allowing them to pass the gap between S. Vicente Spur and Gorringe Bank (the Zenk and Armi (1990) Mediterranean `gateway') as supported by observations. This is not happening in the runs without tidal forcing. Instead, the reduced efficiency in the evacuation of MOW from the GoC results in a gradual salinity increase at MOW depths, which sets up the already mentioned southwestward salt flux. Additional support to our
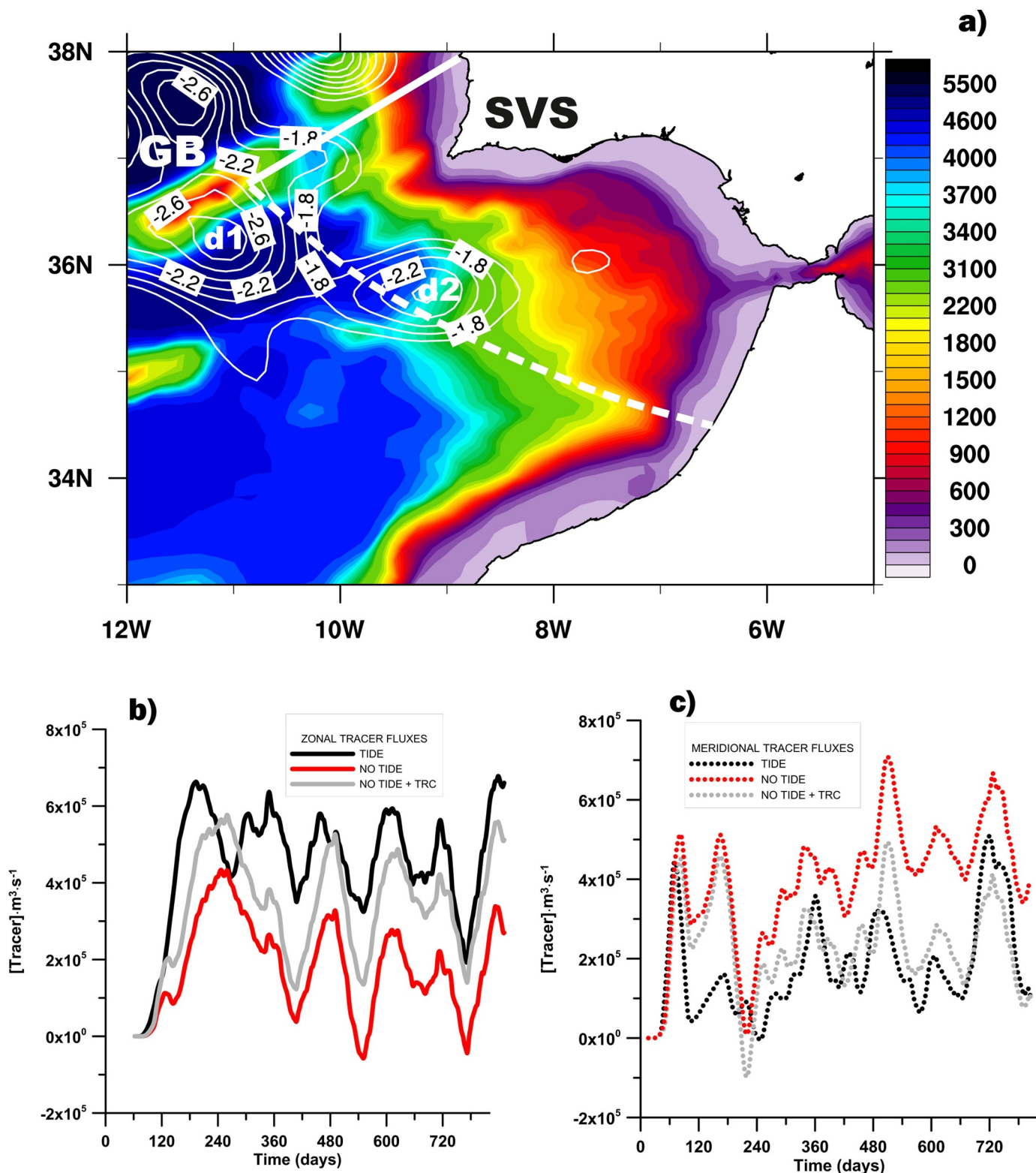
**Fig. 16.** (a) Bathymetry map overlaid with tidal residual SSH contours (d1 and d2 mark lows) with indication of the lines used for tracer transport calculation (white). Also indicated are S. Vicente Spur (SVS) and Gorringe Bank (GB). Tracer transport time series through the northwestern (b) and southwestern (c) boundaries. FSW_TIDE (black), FWS_NOTIDE (red), FWS_NOTIDE + residual tidal velocities (grey).

conclusions is given by the model skills to properly reproduce different aspects of the tidal dynamics in the GoC. The surface tide, tidal currents and internal wave generation and propagation have been satisfactorily compared to observations.

Therefore, to properly understand the impact that local processes acting on MOW in the GoC and the SoG have on the larger scale it is necessary to study the Mediterranean Sea and the North Atlantic Ocean as a unique system accounting for relevant local and small scale
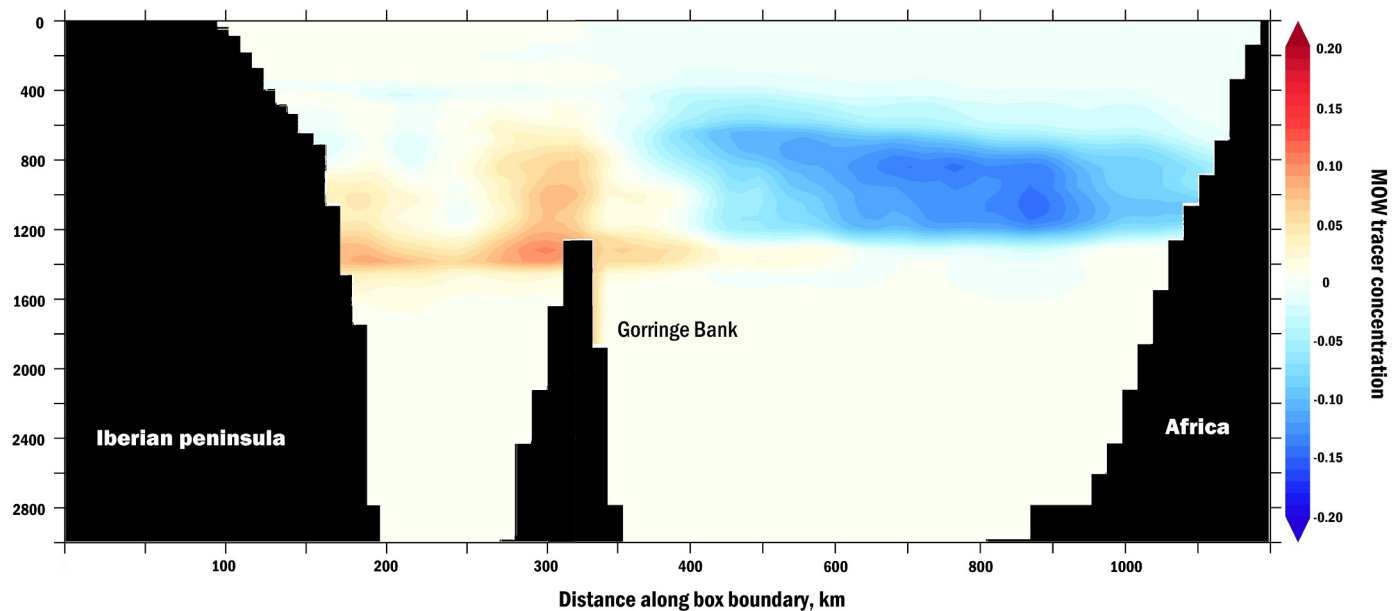
**Fig. 17.** FWS_TIDE-FWS_NOTIDE difference in tracer concentration along de GoC box boundaries (solid and dashed while lines in Fig. 16a). Data averaged over days 366–730 of experiments (see Fig. 16b and c).

processes and also for the atmospheric feedbacks, which is considered as a milestone challenge (Artale et al., 2006; Legg et al., 2009). In all our experiments the tidal runs show a more northward spreading of MOW in comparison to the simulations without tides, which might have implications on the formation of NADW and its variability.

## Supplementary materials

Supplementary material associated with this article can be found, in the online version, at doi:10.1016/j.ocemod.2018.08.003.

## References

Artale, V., Calmanti, S., Sutera, A., 2003. Thermohaline circulation sensitivity to intermediate level anomalies. Tellus 54A, 159–174.

Artale, V., Calmanti, S., Malanotte-Rizzoli, P., Pisacane, G., Rupolo, V., Tsimplis, M., 2006. The Atlantic and Mediterranean Sea as connected systems. In: Lionello, P., Malanotte-Rizzoli, P., Boscolo, R. (Eds.), Mediterranean Climate Variability. Elsevier, Amsterdam, pp. 283–323.

Barbosa, A., Peliz, A., Neves, F., Bashmachnikov, I., Carton, X., 2015. Mediterranean outflow transports and entrainment estimates from observations and high-resolution modelling. Prog. Oceanogr. 131, 33–45.

Baringer, M.O., Price, J.F., 1997. Mixing and spreading of the Mediterranean outflow. J. Phys. Oceanogr. 27 (8), 1654–1677.

Barton, E.D., 1989. The poleward undercurrent on the eastern boundary of the subtropical North Atlantic. In: Neshyba, S., Smith, R.L. (Eds.), Poleward Flows Along Eastern Ocean Boundaries 34. Coastal and Estuarine Studies, Springer-Verlag, New York, pp. 82–95.

Bleck, R., 2002. An oceanic general circulationmodel framed in hybrid isopycnic-cartesian coordinates. *Ocean Model.* 4, 55–88.

Bormans, M., Garrett, C., Thompson, K.R., 1986. Seasonal variability of the surface inflow through the Strait of Gibraltar. Oceanol. Acta 9, 403–414.

Bower, A.S., Serra, N., Ambar, I., 2002. Structure of the Mediterranean undercurrent and Mediterranean water spreading around the Southwestern Iberian Peninsula. J. Geophys. Res. 107 (C10) 25.1–25.19.

Boyer, T.P., Antonov, J.I., Baranova, O.K., Coleman, C., Garcia, H.E., Grodsky, A., Johnson, D.R., Locarnini, R.A., Mishonov, A.V., O'Brien, T.D., Paver, C.R., Reagan, J.R., Seidov, D., Smolyar, I.V., Zweng, M.M., 2013. World Ocean database 2013. Levitus, S., Mishonov, A. (Eds.), World Ocean database 2013. NOAA Atlas NESDIS 72, 209.

Bozec, A., Lozier, M.S., Chassignet, E.P., Halliwell, G.R., 2011. On the variability of the Mediterranean outflow in the North Atlantic from 1948 to 2006. J. Geophys. Res. 106, C09033. https://doi.org/10.1029/2011JC007191.

Brandt, P., Alpers, W., Backhaus, O., 1996. Study of the generation and propagation of internal waves in the Strait of Gibraltar using a numerical model and synthetic aperture radar images of the European ERS-1. J. Geophys. Res. 101, 14237–14252.

Brandt, P., Rubino, A., Sein, D.V., Baschek, B., Izquierdo, A., Backhaus, J.O., 2004. Sea level variations in the western Mediterranean studied by a numerical tidal model of the Strait of Gibraltar. J. Phys. Oceanogr. 34, 433–443.

Bray, N.A., Winant, C.D., Kinder, T.H., Candela, J., 1990. Generation and kinematics of the internal tide in the strait of Gibraltar. In: Pratt, L.J. (Ed.), The Physical Oceanography of Sea Straits. Kluwer, Dordrecht, pp. 477–491 NATO/ASI Series.

Bray, N.A., Ochoa, J., Kinder, T.H., 1995. The role of the interface in exchange through the Strait of Gibraltar. J. Geophys. Res. 100 10 755–10 776.

Bruno, M., Vázquez, A., Gomez-Enri, J., Vargas, J.M., Lafuente, J., Ruiz-Cañavate, A., Mariscal, L., Vidal, J., 2006. Observations of internal waves and associated mixing phenomena in the Portimao Canyon area. Deep-Sea Res. II 53, 1219–1240.

Bryden, H.L., Candela, J., Kinder, T.H., 1994. Exchange through the Strait of Gibraltar. Prog. Oceanogr. 33, 201–248.

Candela, J., Winant, C.D., Bryden, H.L., 1989. Meteorologically forced subinertial flows through the Strait of Gibraltar. J. Geophys. Res. 94, 12667–12679.

Candela, J., Winant, C.D., Ruiz, A., 1990. Tides in the Strait of Gibraltar. J. Geophys. Res. 95, 7313–7335.

Carracedo, L., Gilcoto, M., Mercier, H.PérezF., 2014. Seasonal dynamics in the Azores-Gibraltar Strait region: a climatologically-based study. Prog. Oceanogr. 122, 116–130.

Chen, C., Beardsley, R.C., Limeburner, R., 1995. A Numerical Study of stratified tidal rectification over finite-amplitude banks. Part II: geoges bank. J. Phys. Oceanogr. 25, 2111–2128.

Daniault, N., Maze, J.P., Arhan, M., 1994. Circulation and mixing of Mediterranean water west of the Iberian Peninsula. Deep-Sea Res. I 41, 1685–1714.

Drillet, Y., Bourdallé-Badie, R., Siefridt, L., Le Provost, C., 2005. Meddies in the mercator North Atlantic and Mediterranean Sea eddy-resolving model. J. Geophys. Res. 110, C03016.

Garrett, C., Akerley, J., Thompson, K., 1989. Low-frequency fluctuations in the Strait of Gibraltar from MEDALPEX sea level data. J. Phys. Oceanogr. 19, 1682–1696.

Gary, S.F., Lozier, M.S., Böning, C.W., Biastoch, A., 2011. Deciphering the pathways for the deep limb of the meridional overturning circulation. Deep-Sea Res. II 58, 1781–1797. https://doi.org/10.1016/j.dsr2.2010.10.059.

Gent, P.R., Willebrand, J., McDougall, T.J., McWilliams, J.C., 1995. Parameterizing eddy-induced tracer transports in ocean circulation models. J. Phys. Oceanogr. 25, 463–474.

Griffies, S.M., 1998. The Gent–McWilliams skew-flux. J. Phys. Oceanogr. 28, 831–841.

Iorga, M.C., Lozier, M.S., 1999a. Signatures of the Mediterranean outflow from a North Atlantic climatology 1. Salinity and density fields. J. Geophys. Res. 104, 25985–26009.

Iorga, M., Lozier, M.S., 1999b. Signatures of the Mediterranean outflow from a North Atlantic climatology 2. Diagnostic velocity fields. J. Geophys. Res 104, 26011–26029.

Ivanovic, R.F., Valdes, P.J., Flecker, R., Gregoire, L.J., Gutjahr, M., 2013. The parameterisation of Mediterranean–Atlantic water exchange in the hadley centre model HadCM3, and its effect on modelled North Atlantic climate. *Ocean Model.* 62, 11–16.

Izquierdo, A., Tejedor, L., Sein, D.V., Backhaus, J.O., Brandt, P., Rubino, A., Kagan, B.A., 2001. Control variability and internal bore evolution in the Strait of Gibraltar: a 2-D two-layer model study. Estuarine Coastal Shelf Sci. 53, 637–651.

Jia, Y., Coward, A.C., de Cuevas, B.A., Webb, D.J., Drijfhout, S.S., 2007. A model analysis of the behaviour of the Mediterranean water in the North Atlantic. J. Phys. Oceanogr. 37 (3), 764–786 2007.

Johnson, J., Ambar, I., Serra, N., Stevens, I., 2002. Comparative studies of the spreading of Mediterranean water through the Gulf of Cadiz. Deep-Sea Res. II 49 (19), 4179–4193.

Johnson, J., Stevens, I., 2000. A fine resolution model of the eastern North Atlantic between the Azores, the Canary Islands and the Gibraltar Strait. Deep Sea Res. I 47, 875–899. https://doi.org/10.1016/S0967-0637(99)00073-4.

Jungclaus, J.H., Fischer, N., Haak, H., Lohmann, K., Marotzke, J., Matei, D., Mikolajewicz, U., Notz, D., von Storch, J.S., 2013. Characteristics of the ocean simulations in MPIOM, the ocean component of the MPI-Earth system model. J. Adv. Model. Earth Syst. 5, 422–446.

Jungclaus, J.H., Mellor, G.L., 2000. A three-dimensional model study of the Mediterranean outflow. J. Mar. Syst. 24, 41–66.

Kinder, T.H., Bryden, H.L., 1987. The 1985-1986 Gibraltar experiment: data collection and preliminary results. EOS (Trans. Am. Geophys. Union) 68, 793–794 786-787.

Kurapov, A.L., Allen, J.S., Egbert, G.D., 2010. Combined effects of wind-driven upwelling and internal tide on the continental shelf. J. Phys. Oceanogr. 40, 737–756.

Legg, S., Chang, Y., Chassignet, E.P., Danabasoglu, G., Ezer, T., Gordon, A.L., Griffies, S., Hallberg, R., Jackson, L., Large, W., Ozgökmen, T., Peters, H., Price, J., Riemenschneider, U., Wu, W., Xu, X., Yang, J., 2009. Improving oceanic overflow representation in climate models: the Gravity Current Entrainment Climate Process Team. Bull.Am. Meteorol. Soc. 90, 657–670.

Li, Z., Von Storch, J.-S., Müller, M., 2015. The M2 internal tide simulated by a 1/10° OGCM. J. Phys. Oceanogr. 45, 3119–3135. https://doi.org/10.1175/JPO-D-14-0228.1.

Maas, L.R.M., Zimmerman, J.T.F., 1989. Tide-topography interaction in a stratified shelf sea, II: basic equations for quasinonlinear internal tides. Geophys. Astrophys. Fluid Dyn. 45, 37–69.

Machín, F., Pelegrí, J.L., 2009. Northward penetration of Antarctic Intermediate water off Northwest Africa. J. Phys. Oceanogr. 39, 512–535.

Maier-Reimer, E., 1997. Design of a closed boundary regional model of the Arctic Ocean. In: *Bull. Am. Meteorol. Soc.*: Workshop on polar processes in global climate, 13–15 Nov, 1996, pp. 72–73.

Marsland, S.J., Haak, H., Jungclaus, J.H., Latif, M., Röske, F., 2003. The Max Planck Institute global ocean/sea ice model with orthogonal curvilinear coordinates. *Ocean Model.* 5, 91–127.

Morozov, E.G., Trulsen, K., Velarde, M.G., Vlasenko, V.I., 2002. Internal tides in the Strait of Gibraltar. J. Phys. Oceanogr. 32, 3193–3206.

Müller, M., Cherniawsky, J.Y., Foreman, M.G.G., von Storch, J.-S., 2012. Global M2 internal tide and its seasonal variability from high resolution ocean circulation and tide modeling. Geophys. Res. Lett. 39, L19607. https://doi.org/10.1029/2012GL053320.

Müller, M., Haak, H., Jungclaus, J.H., Sündermann, J., Thomas, M., 2010. The effect of ocean tides on a climate model simulation. *Ocean Model.* 35, 304–313.

Musgrave, R.C., MacKinnon, J.A., Pinkel, R., Waterhouse, A.F., Nash, J., Kelly, S.M., 2017. The influence of subinertial internal tides on near-topographic turbulence at the mendocino ridge: observations and modeling. J. Phys. Oceanogr. 47, 2139–2154. https://doi.org/10.1175/JPO-D-16-0278.1.

Ochoa, J., Bray, N.A., 1991. Water mass exchange in the Gulf of Cadiz. Deep Sea Res., Part A 38 (suppl. 1), S465–S503.

Pacanowski, R.C., Dixon, K., Rosati, A., 1990. The GFDL Modular Ocean Model Users guide: Version 1.0 GFDL Group Technical Rept No. 2, Geophysical Fluid Dynamics Laboratory/NOAA. Princeton Univ, Princeton, NJ.

Pacanowski, R.C., Philander, G.H., 1981. Parameterization of vertical mixing in numerical models of tropical oceans. J. Phys. Oceanogr. 11, 1443–1451.

Papadakis, M.P., Chassignet, E.P., Hallberg, R.W., 2003. Numerical simulations of the Mediterranean Sea outflow: impact of the entrainment parameterization in an isopycnic coordinate model. *Ocean Model.* 5, 325–356.

Peliz, A., Boutov, D., Cardoso, R.M., Delgado, J., Soares, P., 2013. The Gulf of Cadiz-Alboran Sea sub-basin: model setup, exchange and seasonal variability. Ocean Model. 61, 49–67.

Peliz, A.J.Dubert, Marchesiello, P., Teles-Machado, A., 2007. Surface circulation in the Gulf of Cadiz: model and mean flow structure. J. Geophys. Res. 112, C11015.

Price, J.F., Baringer, M.O., 1994. Outflows and deep water production by marginal seas.

Prog. Oceanogr. 33, 161–200.

Quaresma, L., Pichon, A., 2013. Modelling the barotropic tide along the West-Iberian margin. J. Mar. Syst. 109–110, S3–S25.

Richardson, P.L., McCartney, M.S., Maillard, C., 1991. A search for meddies in historical data. Dyn. Atmos. Oceans 15, 241–265.

Röske, F., 2001. An atlas of surface fluxes based on the ECMWF re-analysis – a climatological dataset to force global ocean general circulation models. MPI für Meteorol., Rep. 323, 31.

Sánchez-Garrido, J.C., Sannino, G., Liberti, L., Garcia Lafuente, J., Pratt, L.J., 2011. Numerical modelling of three-dimensional stratified tidal flow over Camarinal Sill, Strait of Gibraltar. J. Geophys. Res. 116, C12026. https://doi.org/10.1029/2011JC007093.

Sánchez-Garrido, J.C., Garcia-Lafuente, J., Criado-Aldeanueva, F., Baquerizo, A., Sannino, G., 2008. Time-spatial variability observed in velocity of propagation of the internal bore in the Strait of Gibraltar. J. Geophys. Res. 113, C07034. https://doi.org/10.1029/2007JC004624.

Sánchez-Leal, R.F., Bellanco, M.J., Fernández-Salas, L.M., García-Lafuente, J., Gasser-Rubinat, M., González-Pola, C., Hernández-Molina, F.J., Pelegrí, J.L., Peliz, A., Relvas, P., Roque, D., Ruiz-Villarreal, M., Sammartino, S., Sánchez-Garrido, J.C., 2017. The Mediterranean overflow in the Gulf of Cadiz: a rugged journey. Sci. Adv. 3, eaao0609.

Sannino, G., Bargagli, A., Artale, V., 2002. Numerical modeling of the mean exchange through the Strait of Gibraltar. J. Geophys. Res. 107 (C8), 3094. https://doi.org/10.1029/2001JC000929.

Sannino, G., Bargagli, A., Artale, V., 2004. Numerical modeling of the semidiurnal tidal exchange through the Strait of Gibraltar. J. Geophys. Res. 109, C05011. https://doi.org/10.1029/2003JC002057.

Sannino, G., Carillo, A., Pisacane, G., Naranjo, C., 2015. On the relevance of tidal forcing in modelling the Mediterranean thermohaline circulation. Prog. Oceanogr. 134, 304–329.

Seidler, G., 1968. haufigkeitsverteil von wasserarten im ausstrombereich von meeresstrassen. Kiel. Meeresforch. 24 (2), 59–65.

Sein, D.V., Mikolajewicz, U., Gröger, M., Fast, I., Cabos, W., Pinto, J.G., Hagemann, S., Semmler, T., Izquierdo, A., Jacob, D., 2015. Regionally coupled atmosphere-ocean-sea ice-marine biogeochemistry model ROM: 1. description and validation. J. Adv. Model. Earth Syst. 7, 268–304.

Serra, N., Ambar, I., Kase, R., 2005. Observations and numerical modelling of the Mediterranean outflow splitting and eddy generation. Deep Sea Res. II 52, 383–408.

Serra, N., Ambar, I., Boutov, D., 2010. Surface expression of Mediterranean water dipoles and their contribution to the shelf/slope–open ocean exchange. Ocean Sci. 6, 191–209.

Steele, M., Morley, R., Ermold, W., 2001. PHC: a global ocean hydrography with a high quality Arctic Ocean. J. Clim. 14, 2079–2087.

Sweby, P.K., 1984. High resolution schemes using flux-limiters for hyperbolic conservation laws. SIAM J. Numer. Anal. 21, 995–1011.

Taguchi, E., Stammer, D., Zahel, W., 2014. Inferring deep ocean tidal energy dissipation from the global high-resolution data-assimilative HAMTIDE model. J. Geophys. Res. Oceans 119, 4573–4592. https://doi.org/10.1002/2013JC009766.

Tejedor, L., Izquierdo, A., Sein, D.V., Kagan, B.A., 1998. Tides and tidal energetics of the Strait of Gibraltar: a modelling approach. Tectonophysics 294, 333—347.

Tejedor, L., Izquierdo, A., Kagan, B.A., Sein, D.V., 1999. Simulation of the semidiurnal tides in the Strait of Gibraltar. J. Geophys. Res. 104 (C6), 13541–13557.

Thomas, M., Sündermann, J., Maier-Reimer, E., 2001. Consideration of ocean tides in an OGCM and impacts on subseasonal to decadal polar motion excitation. Geophys. Res. Lett. 28, 2457–2460.

Treguier, A.M., Talandier, C., Theetten, S., 2003. Modelling Mediterranean water in the North-East Atlantic. lab. de physique des oceans, rapport interne, LPO 02-14.

Vlasenko, V., Sanchez Garrido, J.C., Stashchuk, N., Garcia Lafuente, J., Losada, M., 2009. Three-Dimensional evolution of large-amplitude internal waves in the Strait of Gibraltar. J. Phys. Oceanogr. 39, 2230–2246.

Wang, D.P., 1993. The Strait of Gibraltar Model: internal tide, diurnal inequality and fortnightly modulation. *Deep-Sea Res.* 40, 1187—1203.

Weber, T., Thomas, M., 2017. Influence of ocean tides on the general ocean circulation in the early Eocene. Paleoceanography 32, 553–570. https://doi.org/10.1002/2016PA002997.

Xu, X., Chassignet, E.P., Price, J.F., Ozgökmen, T.M., Peters, H., 2007. A regional modeling study of the entraining mediterranean outflow. J. Geophys. Res. 112, C12005.

Zenk, W., Armi, L., 1990. The complex spreading pattern of Mediterranean water off the Portuguese continental slope. *Deep-Sea Res.* 37, 1805–1823.

Zweng, M.M, Reagan, J.R., Antonov, J.I., Locarnini, R.A., Mishonov, A.V., Boyer, T.P., Garcia, H.E., Baranova, O.K., Johnson, D.R., Seidov, D., Biddle, M.M., 2013. In: Levitus, Salinity.S. (Ed.), World Ocean Atlas 2013 2. A. Mishonov Technical Ed., pp. 39 NOAA Atlas NESDIS 74.